THE DESIGN AND CONSTRUCTION OF A MODIFIED GRAMME-RING ARMATURE FOR A GENERATOR WITH A SUPERCONDUCTING FIELD WINDING

by

Craig G. Prohazka

B.S. Rensselaer Polytechnic Institute

(1975)

Submitted in Partial Fulfillment of the Requirements
For the Degree of Master of Science

at the

Massachusetts Institute of Technology

May, 1977

Signature of Author ______________________

Department of Electrical Engineering, May 19, 1977

Certified by ______________________

Thesis Supervisor

Accepted by ______________________

Chairman, Department Committee on Graduate Students

DESIGN AND CONSTRUCTION OF A MODIFIED GRAMME-RING ARMATURE FOR A GENERATOR WITH A SUPERCONDUCTING FIELD WINDING

by

Craig G. Prohazka

Submitted to the Department of Electrical Engineering on May 19, 1977, in partial fulfillment of the requirements for the degree of Master of Science.

ABSTRACT

The use of a modified Gramme-Ring armature with a superconducting field winding allows high terminal voltage with a reasonable insulation requirement. Such an armature is constructed for operation with a previously fabricated rotor. Important parameters of the armature are measured and compared with the predictions of a theoretical analysis. Special attention is given to the sources of power loss. It is concluded that the theoretical analysis accurately predicts the performance of the armature.

Thesis Supervisor: James L. Kirtley, Jr.

Title: Assistant Professor of Electrical Engineering

TABLE OF CONTENTS

LIST OF FIGURES page

LIST OF TABLES

GLOSSARY OF SYMBOLS

Subscripts:

a	armature winding
a	phase A
b	phase B
c	phase C
c	core
d	direct axis
f	field winding
i	inner
o	outer
s	image shield

Symbols

B	magnetic flux density
d_c	core loss per unit mass
d_w	armature wire diameter
E_f	voltage behind synchronous reactance
c	heat capacity
C_1	constant used in P_{sh} calculation
C_2	constant used in P_{sh} calculation
C_{mn}	geometric factor in field-to-armature mutual
C_{xi}	geometric factor used in armature self inductance
C_{xo}	geometric factor used in armature self inductance

H	magnetic field intensity
i	current
I_a	rated armature terminal current (RMS)
I_{ph}	rated armature phase current (RMS)
I_{ph_b}	rate armature phase belt current (RMS)
J	current density
Ja	rated armature current density
K	surface current density
ℓ	straight section length
ℓ_a	armature length for self inductance
ℓ_m	length for field-to-armature mutual inductance
L_a	armature self inductance
L_{ab}	armature phase-to-phase mutual inductance
L_f	field self inductance
M	armature-to-field mutual inductance (for two parallel connected armature windings)
N_{at}	number of armatures turns per phase belt
N_{ft}	number of turns in field winding
P_c	core loss
P_{ec}	armature eddy-current loss
P_{sh}	magnetic shield dissipation
Q	heat
r	radius
R	radius (current sheets)
R_{fi}	field winding inner radius
R_{fo}	field winding outer radius

R_{aii}	inner armature inner radius
R_{aoi}	inner armature outer radius
R_{ci}	core inner radius
R_{aio}	outer armature inner radius
R_{aoo}	outer armature outer radius
R_s	image shield inner radius
R_{DC}	armature D.C. resistance
R_{AC}	armature A.C. resistance
t	time
t	temperature
t_c	core thickness
V	volume
$\underline{s}$	surface coefficient
X	reactance (ohms)
X_a	synchronous reactance (ohms)
x_a	per unit synchronous reactance normalized to E_f
x_d	per unit synchronous reactance
$x_i=R_{aii}/R_{aoi}$	inner armature radius ratio
$x_o=R_{aio}/R_{aoo}$	outer armature radius ratio
$y=R_{fi}/R_{fo}$	field radius ratio
$z=(R_{co}/R_s)^2$	boundary radius ratio (outer armature)

<u>Greek symbols:</u>

β	wave number
Γ_i	inner reflection coefficient
Γ_o	outer reflection coefficient
δ	skin depth
ϵ	permittivity
θ	angular measure
θ_{wfe}	field winding angle
θ_{wae}	armature winding angle
λ	flux linkage
λ_p	armature packing factor
μ	permeability
ρ	resistivity
ρ	mass density
ρ_c	core mass density
σ	conductivity
τ	time
ψ	power factor angle
ω	angular frequency

INTRODUCTION

This thesis is a report on an experimental superconducting generator which has an armature of a new configuration. The objective of this investigation was to study the properties of this type of armature design, the modified Gramme-Ring armature.(1) An armature of this type was built and tested as part of a superconducting generator using the rotor from an earlier experiment.(2,3,4,5) Results of tests performed on this machine are compared with earlier theoretical results.(6) It is concluded that the theoretical analysis accurately predicts the performance of the armature. Further, the sources of armature power loss are located, and the contribution of each is calculated or measured experimentally or both. Although the total loss is higher than at first hoped, improvements in design are suggested.

One of the advantages proposed for superconducting machines is the possibility of generating electric power at very high voltages, perhaps even at transmission levels. In contrast, conventional large alternators have a maximum economic terminal voltage on the order of 24 to 32 kV. Consequently, terminal currents in these alternators are extremely large, requiring expensive and lossy bushings and buses, as well as unit transformers of high rating to convert the power to transmission levels.

An alternator with terminal voltage at transmission level would not need much of this expensive terminal equipment, and would have other advantages. First, the power loss in the transformer and the buses would be eliminated. Also, a system without these elements would be simpler and consequently might be more reliable. In addition, the elimination of transformer leakage reactance could improve the system stability, or it could allow an increase in machine reactance, resulting in higher machine power density and lower terminal fault currents. Further, controlled gradient windings will have greatly improved performance during switching surges, and a much higher ability to withstand fast rise time overvoltage conditions. The development of alternators with terminal voltage significantly above that now economically feasible, but below transmission levels, would yield some of the advantages but to a lesser degree.[7]

The need for a high permeability magnetic circuit in conventional turbine generators requires that the stator core have teeth. Consequently, the space available to armature conductors is limited to spaces between the teeth. Further, each conductor must be insulated for full machine potential. This results in a poor space factor, since both the insulation and stator teeth take up space. Also, because the electrical insulation is a poor heat tranfer medium, either a low copper current density or some form of internal conductor cooling is required. The former results in a low power density, the latter in rather complex plumbing.

The application of superconductors to the field windings of turbine generators results in the capability of an extremely high magnetomotive force. Consequently, unlike conventional generators, a high permeability magnetic circuit is not required. There are several ways a designer of armatures for superconducting generators can take advantage of this fact.

First, he might choose to eliminate all iron from the armature. This configuration was chosen for the second experimental superconducting machine built at MIT.[8] In the straight section, conductors need be insulated only from neighboring conductors. In other words, the insulation need only be thick enough to withstand turn-to-turn potential. However, in the end turn region, conductors of strongly different potential must cross. Fortunately, the resulting potential may be taken across cylindrical insulations.

A second possibility available to the designer eliminates the end turn problem mentioned above by using a toroidal armature. In this case, the conductors are wound around on annular ferromagnetic core, following a path through the central hole and back along the outside. As a result, all conductors which are physically close to one another are also electrically close to one another, even in the end turn region. The function of the ferromagnetic core is to increase armature to field coupling. This form of winding is the same as that of a Gramme-Ring winding and in fact the Gramme-Ring is one of this class. The Gramme-Ring winding, is a continuous toroidal coil, with n taps, where n is the number of phases. It was once used for DC motors, in which case n is large. For small values of n (3, for example), the Gramme-Ring is not a particularly good winding, for two reasons. One is the poor breadth factor caused by 120° phase belts. The other is the possibility of unbalanced armature currents causing side loadings on the rotor.

A modification of the basic Gramme-Ring winding may be made to correct both of these deficiencies at once. The winding is split into six phase belts (for a 3 phase machine), alternate phase belts being wound with opposite sense around the core, as illustrated in figures 1 and 2. Opposing phase belts are connected in parallel to form phase windings. This gives a better breadth factor, as well as eliminating side forces. This configuration is known as the modified Gramme-Ring winding.[7]

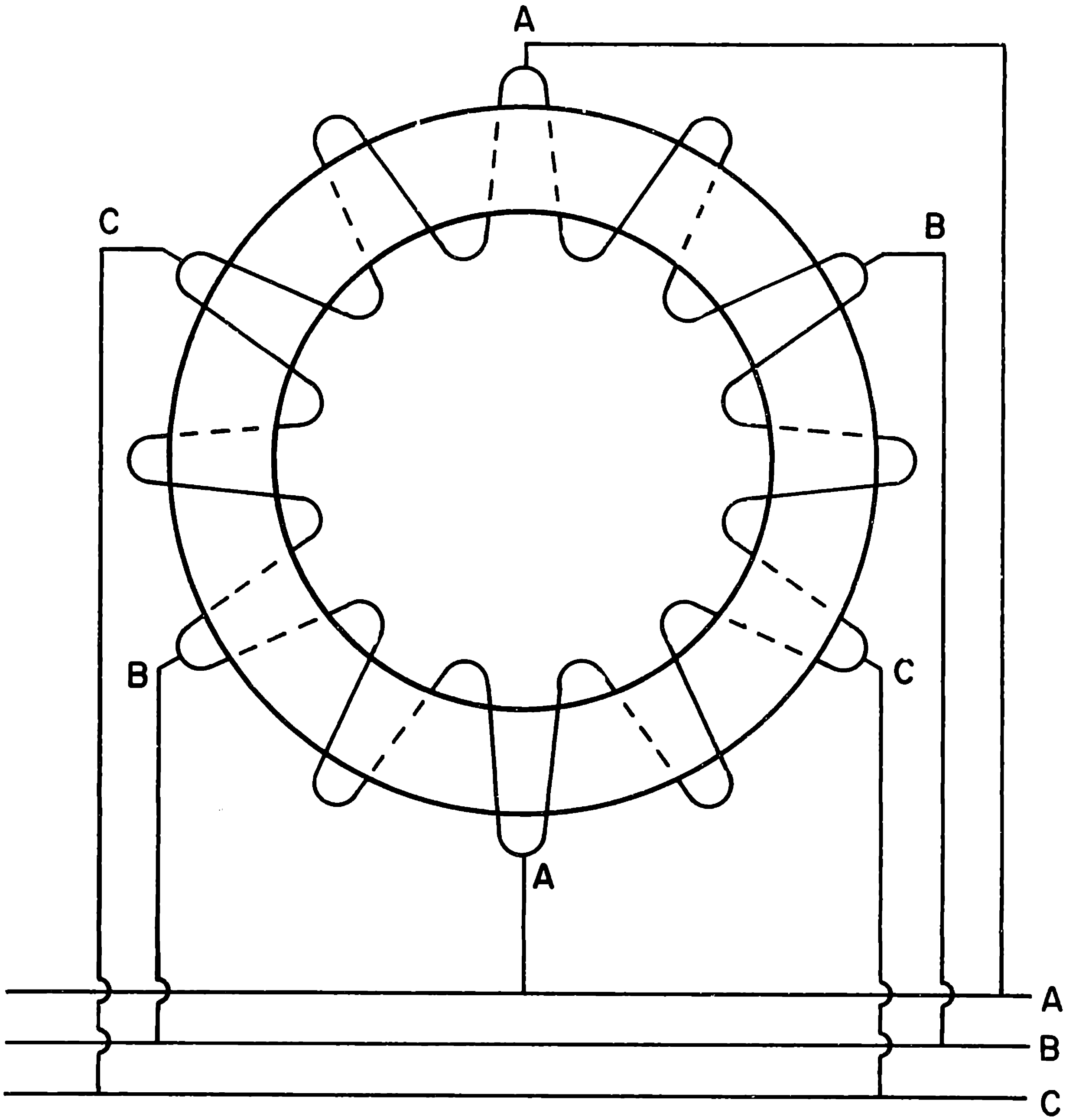

Figure 1: Schematic of Modified Gramme-Ring Winding

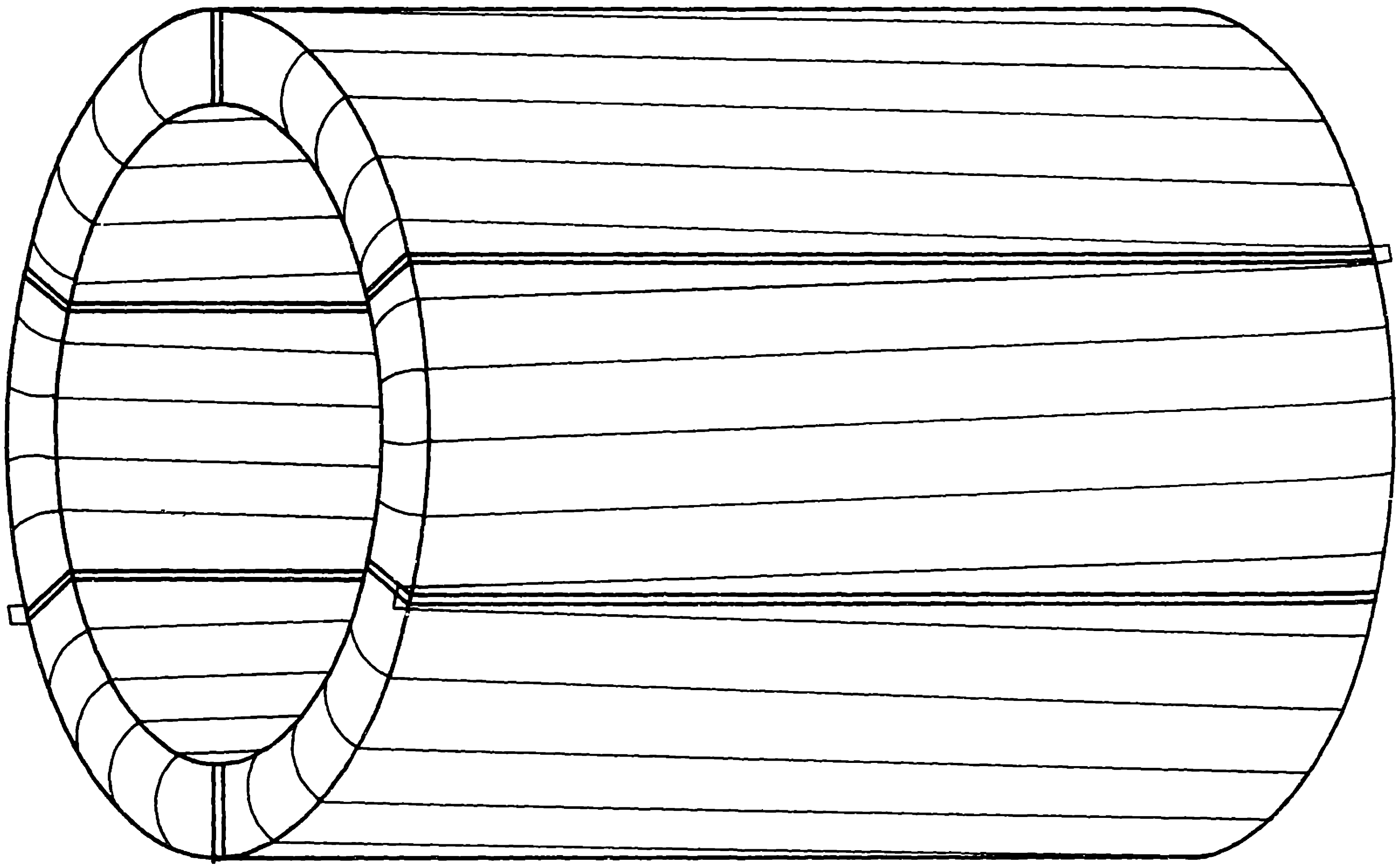

Figure 2: Schematic of Modified Gramme-Ring Winding

Shown in figure 3 is the entire generator assembly. The main components are the armature, rotor, and drive motor.

Drive Motor

The drive motor is a 10 horsepower DC motor with a compound field winding. The motor was run separately excited. The parallel winding is driven by a 120 volt DC source. The armature was supplied by a variable voltage DC supply composed of a variable auto-transformer and rectifier combination.

Rotor

The important features of the rotor are shown in figure 4. The field winding is suspended by a thin, walled, large radius torque tube, to allow maximum strength with minimum conductive heat transfer. The torque tube is vapor cooled by helium from the field winding, flowing up through the gap between the neck plug and the inner shell. Baffles are located in this region to reduce the extent of natural convection loops. The torque tube is strengthened against buckling under pressure from helium vapor in the gap by four support rings. The field winding is further insulated by vacuum to reduce convective heat transfer. Moreover, in the vacuum space is a copper shield to reduce heat transfer by radiation.

The rotor was constructed as part of an earlier experimental supperconducting machine.[2,3,4,5] Unfortunately, at some time during its past operation the rotor was damaged,

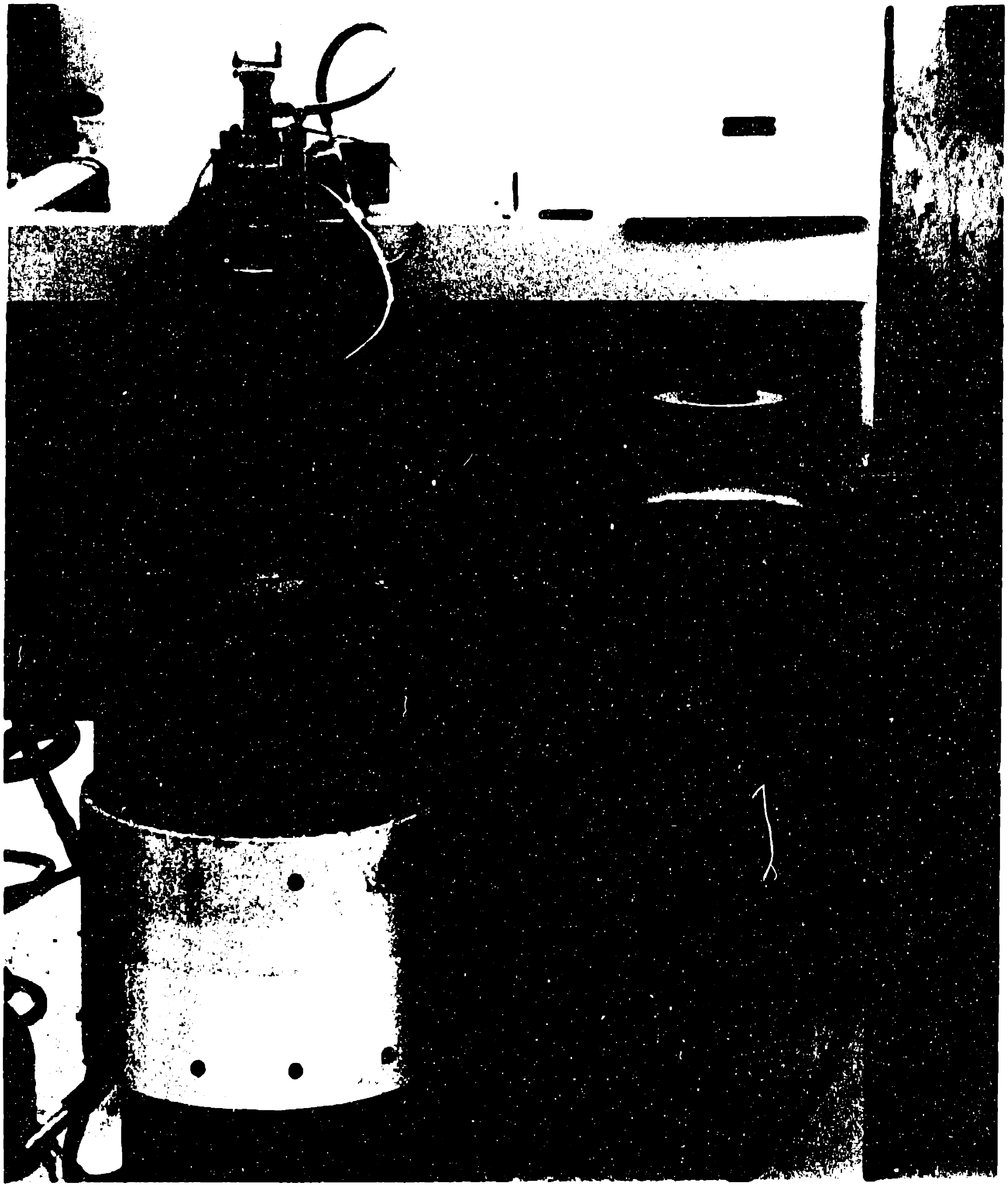

Figure 3: Generator Assembly

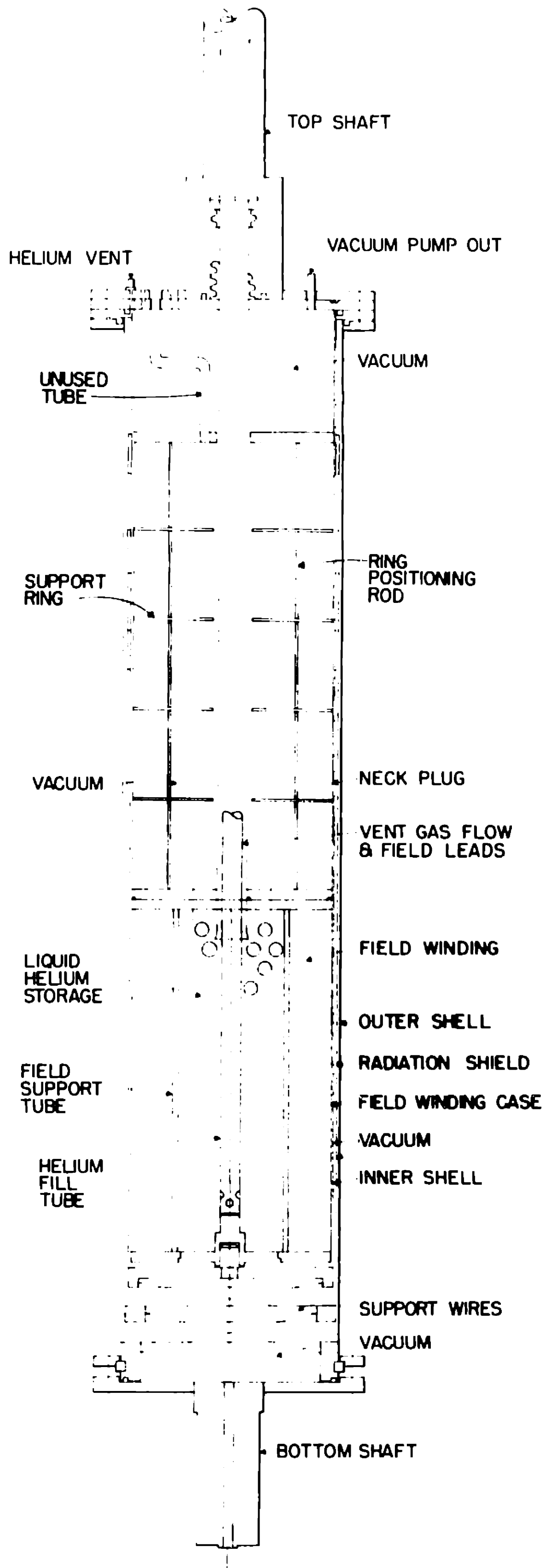

Figure 4: Rotor Configuration After Modification

apparently by a quench. Specifically, we believe the neck plug was crushed by high pressure helium vapor excaping around it. Figure 5 shows the damaged region. In addition to repairing the damage, we redesigned the neck plug to prevent similar problems in the future. The earlier design is shown in figure 6. One obvious difference is the absence of the support rings. Another is the presence of a reservoir of liquid nitrogen located along a portion of the torque tube. Any heat flow down the axis of the rotor was absorbed by the vaporization of liquid nitrogen instead of liquid helium. Other modifications include the blocking off of the nitrogen fill and vent tubes, and the welding of the stainless steel can enclosing the field winding to the field support. Previously, it had been glued. The weld ensures the containment of liquid helium in the field winding area.

Armature

Electrical Description

Many of the dimensions of the armature were fixed a priori, since the rotor and the stator core had already been constructed.

From the start, there were certain restrictions on electrical characteristics. Specifically, the armature is designed to be dual-purpose: it will also be used, with the same rotor as a variable speed, commutatorless superconducting motor utilizing an SCR switching scheme developed at MIT.[9] So, the number of turns per winding and the number

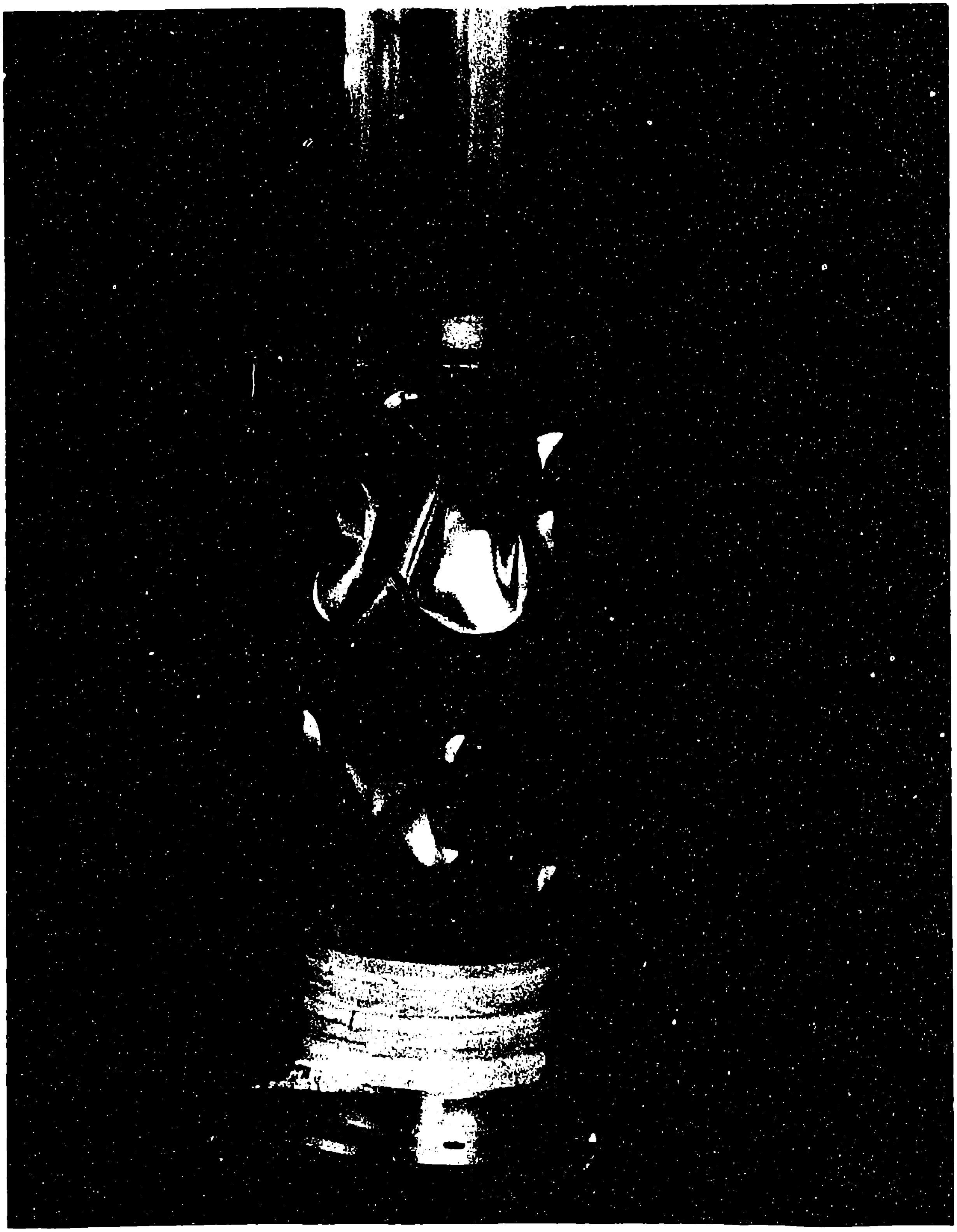

Figure 5: Damaged Neck Plug

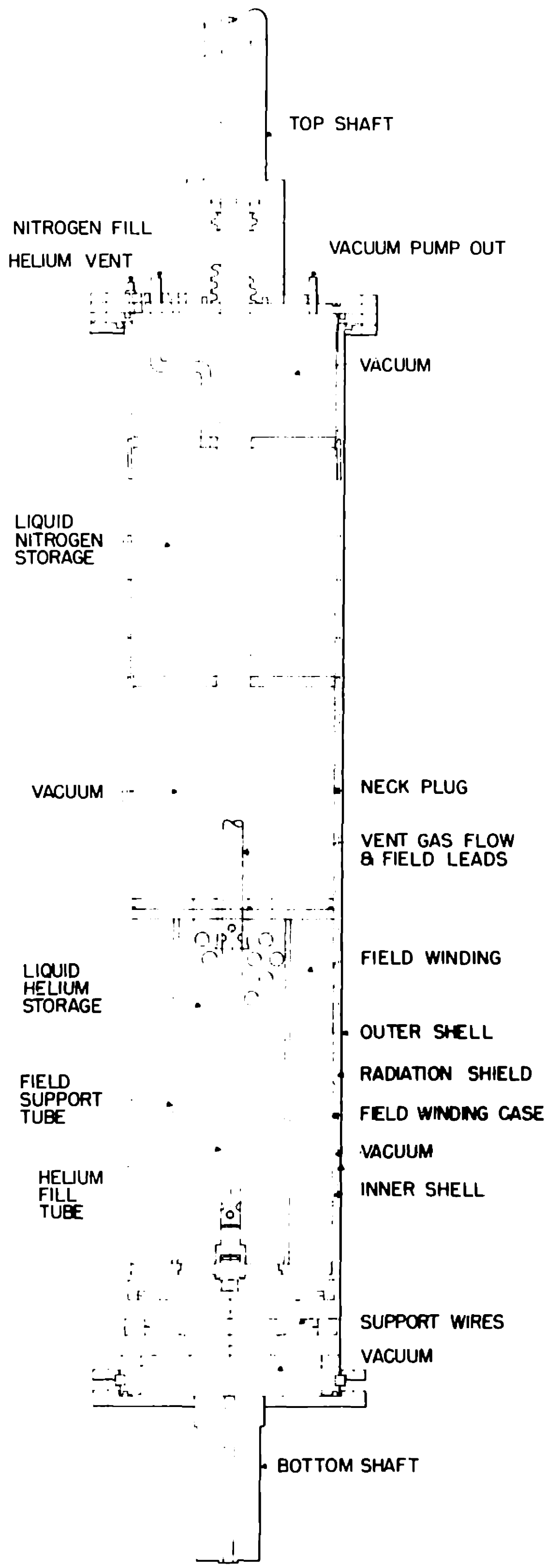

Figure 6: Original Rotor Configuration

Table 1

Dimensions of Armature

Stator inner radius	3.0	in.
Inner armature inner radius	3.25	in.
Inner armature outer radius	5.14	in.
Core inner radius	5.5	in.
Core outer radius	8.25	in.
Thickness of core rings	.656	in.
Core insulation thickness	.050	in.
Outer armature inner radius	8.3	in.
Outer armature outer radius	9.0	in.
Shield inner radius	10.0	in.
Shield outer radius	10.75	in.
Axial length of shield	15.125	in.
Axial length of armature winding	7.5	in.
Axial length of core	4.5	in.

of windings was constrained to be appropriate to both applications. Since the area available to armature conductors is also fixed, the required area of the conductor can be calculated.

The levels of eddy- and circulating-current losses are of fundamental importance in designing the conductor for this machine. First, since the armature has no core teeth to shield the conductors from the air gap magnetic field, it is clear that the conductor primary filament size must be considerably smaller than that customarily used in large machines. Second, these filaments must be well transposed to avoid circulating current loss.

For the above reasons, the conductor configuration chosen is a bundle of seven filaments of number 19 round wire (.036 inches in diameter). Further, the filaments are twisted around one another with a pitch of about an inch and so are well transposed. Each filament is insulated with a .0015 inch layer of Nylese (Phelps-Dodge tradename) solderable insulation.

As previously described, the modified Gramme-Ring configuration suggests that the two phase belts comprising each phase be wound in opposite senses, because the fluxes are in opposite directions. Instead, 23 windings were wound in the same sense, while one ended up in the opposite sense. To compensate for the opposite flux directions, the terminal connections of the windings comprising the appropriate phase belts were simply reversed, as shown in figure 7.

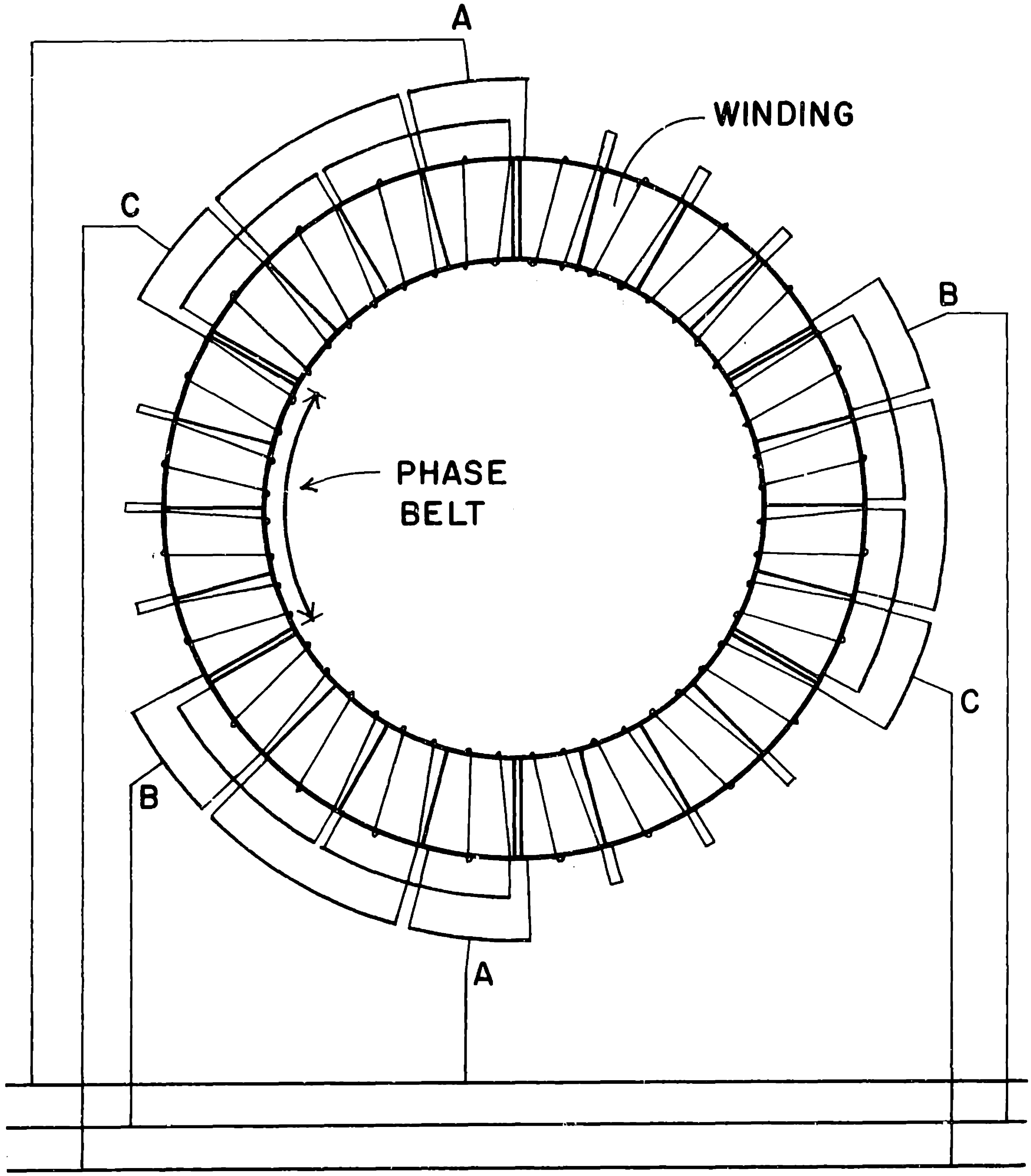

Figure 7: Armature Terminal Connections

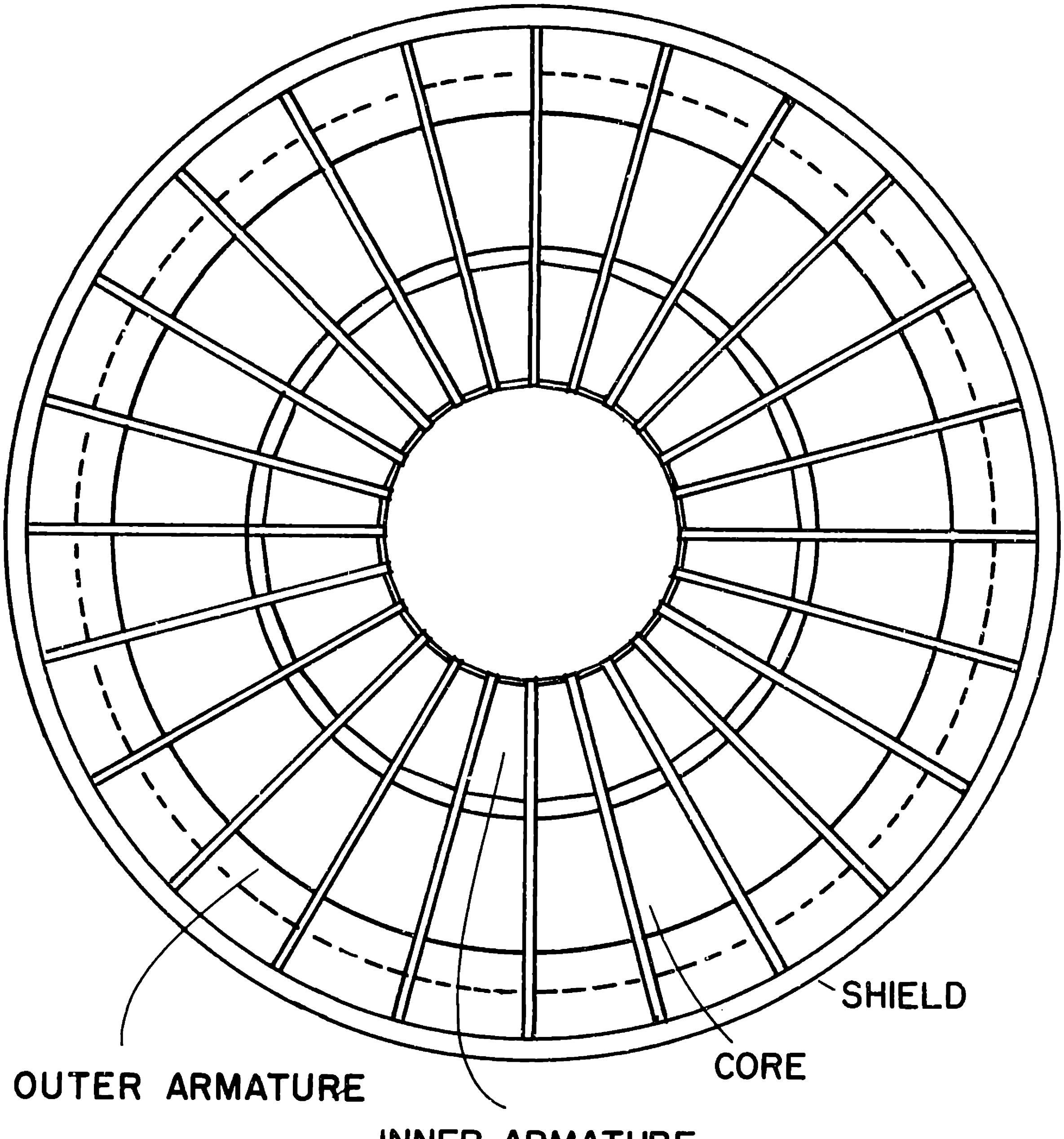

Figure 8: Section Through Armature, Viewed From Above

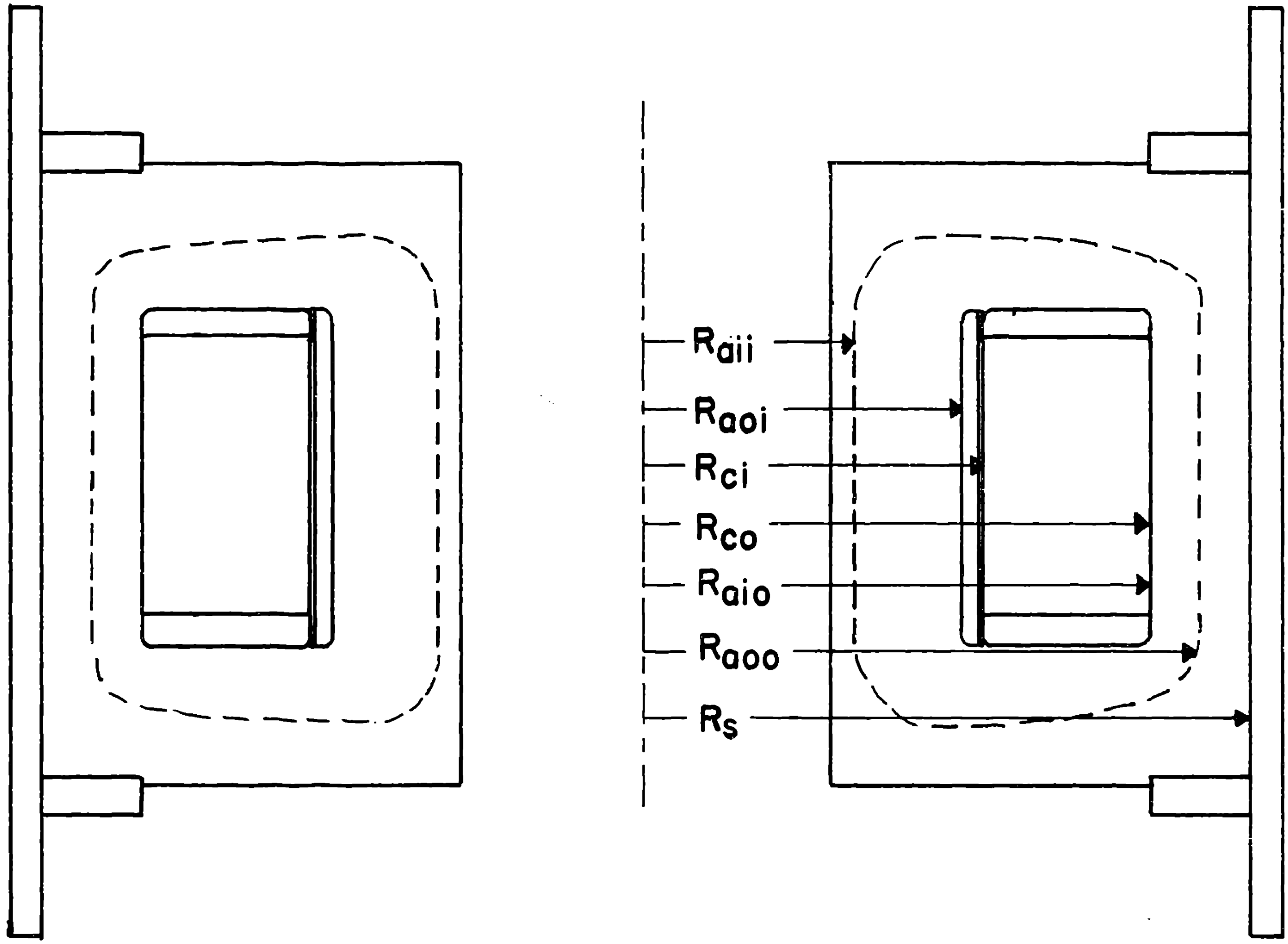

Figure 9: Section Through Armature, Side View

From earlier theoretical results,[6] predictions of the performance of the armature are made. In appendix 1, the shield power loss is calculated. These results are summarized in Table 2.

Specifically, in the self inductance of each armature phase, was calculated from[6]

$$L_a = \frac{16 l_a \mu_0 N_{at}^2 \sin^2(\theta_{wae}/2)}{-3\pi \theta_{wae}^2} \left[\frac{C_{xi}}{(1-x_i^2)^2} + \frac{C_{xo}}{(1-x_o^2)^2(1+z)} \right]$$

where

$$C_{xi} = -1 + 4x_i^3 - 3x_i^4 - \frac{2}{3}(1-x_i^3)^2\left(\frac{R_{aoi}}{R_{ci}}\right)^2$$

and

$$C_{xo} = (1+z)(1-x_o^4) + \frac{2}{3}(1-x_o^3)^2\left(\frac{R_{aoo}}{R_s}\right)^2 - 2(1-x_o^3)(1+zx_o)$$
$$-6(1-x_o^2)\left(\frac{R_{co}}{R_{aoo}}\right)^2 + 2(1-x_o)(x_o^3+z)$$

Lab, the mutual inductance between phases, was determined from

$$L_{ab} = -\frac{1}{2}L_a$$

M, the peak armature to field mutual inductance is found from

$$M = \frac{32 l_m \mu_0 N_{ft} N_{at} C_{mn}}{\pi \theta_{ufe} \theta_{wae} (1-y^2)(1-x_i^2)} \left(\frac{R_{fo}}{R_{aii}}\right)$$

where

$$C_{mn} = \frac{\sin(\theta_{wae}/2)\sin(\theta_{wfe}/2)(1-y^3)}{3}\left[1-x_i+\frac{1}{3}(1-x_i^3)\left(\frac{R_{aoi}}{R_{ci}}\right)^2\right]$$

x_d, the synchronous reactance, was evaluated from

$$x_d = \frac{3}{2}\omega L_a$$

The eddy current power loss is predicted from[6]

$$P_{ec} = \frac{3\theta_{wae}R_{aoi}^2(1-x_i^2)\omega^2\sigma\lambda_p l_{ec} d_w^2(B_{aoi}^2+B_{aio}^2)}{32}$$

where B_{aoi}^2 and B_{aio}^2 are the mean squared flux densities in the inner and outer armatures respectively. The core power loss is calculated by

$$P_c = \pi(R_{co}^2 - R_{ci}^2) l\, d_c \rho_c$$

where d_c is the loss per unit mass, and ρ_c is the mass density. The shield power is shown in appendix 1 to be

$$P_{sh} = \int_V \frac{|\underline{J}|^2}{2}\rho\, dV$$

where $$\underline{J} = \frac{k}{\mu_0}\left(\beta - \frac{\alpha^2}{\beta}\right)\underline{C}_1\left(e^{\alpha y} + \underline{a}e^{-\alpha y}\right)e^{j(\omega t - \beta x)}$$

and α, β, and $\underline{C}_1$ are defined and evaluated in the appendix. The open circuit terminal voltage is calculated from

$$E_f = \frac{\omega M I_f}{2\sqrt{2}}$$

The current rating of the armature is determined by the rule of thumb that the current density in a winding cooled by unforced air be less than 1 x 10^6 amperes/meter^2. The current density related to phase belt current by

$$J_a = \frac{2 N_{at} I_{pbb}}{\theta_{wae} (R_{aoi}^2 - R_{aii}^2)}$$

$$I_{ph} = 2 I_{phb}$$

$$I_L = \sqrt{3}\, I_{ph}$$

The per unit impedance base is determined as follows.

$$P_B = 3 V_{LL_B} I_{ph_B}$$

where V_{LL_B} is the line-to-line rated terminal voltage, and I_{ph_B} is the rated phase current. Further, for the delta configuration,

$$Z_B = \frac{V_{LL_B}}{I_{ph_B}}$$

$$= \frac{P_B}{3 I_{ph_B}^2}$$

In following sections, P_B and I_{ph} are shown to be 37 kVA and 27 amps, respectively. Therefore,

$$Z_B = 16.9 \quad \text{ohms} \quad (\Delta)$$

Table 2

Parameters Used in Theoretical Calculations

Quantity	Symbol	Value
Armature length for self inductance	ℓ_a	.114 meter
Turns per armature phase belt	N_{at}	372
Angle subtended by armature phase belt	θ_{wae}	60°
Armature length for mutual inductance	ℓ_m	.114 meter
Turns in field winding	N_{ft}	5500
Angle subtended by field winding	θ_{wfe}	129°
Conductivity of copper	σ	5.82×10^7 mho/meter
Packing factor	λ_p	.447
Armature length for eddy current loss	ℓ_{ec}	.191 meters
Diameter of armature conductor filament	d_w	.000911 meters
Mass density of core material	ρ_c	7.65 grams/cc
Synchronous reactance	X_a	13.1 ohms per phase (Δ)

Mechanical Description

The modified Gramme-Ring armature is an air gap winding. There are no iron teeth to support the armature conductors against torque. This function is performed by 24 supports made of thermosetting laminate of the continuous filament glass cloth type with epoxy resin binder (NEMA grade G-10). This material has Westinghouse trade-name Micarta. Illustrated in figures 10 and 11, these supports also suspend the core from the outer shield. Since the core is completely covered with insulation, thre is no direct mechanical coupling between the core and the supports. Instead, the core simply rests in the supports, being held in place by friction between the supports and insulation, as well as by friction between the conductors and insulation. Each support surrounds the core. This arrangement is made possible by constructing the support of 2 pieces, as illustrated in figure 12. The pieces are bonded togehter with a tongue-in-groove epoxy joint. The epoxy and curing agent used had the Shell Chemical tradenames Epon Resin 826 and Epon Curing Agent U. The outer corners of the supports are placed in slots in 2 rings, one above and one below. The rings are in turn bolted to the shield. Torque on the armature is transmitted through the supports to the rings, and then to the shield. Figures 13 and 14 show this arrangement, without the core in position. Only the C-shaped support pieces are included.

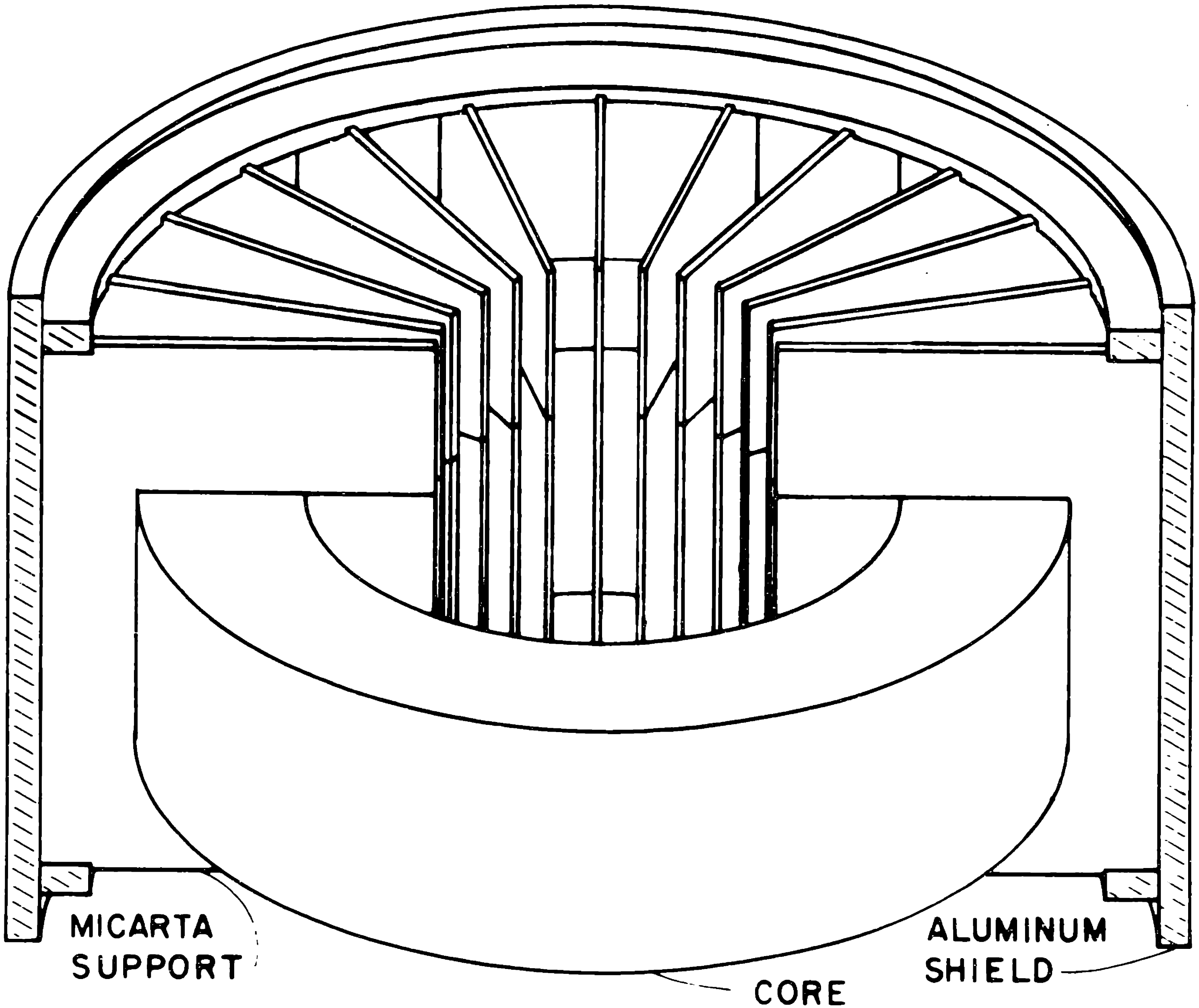

Figure 10: Armature Cutaway Vi

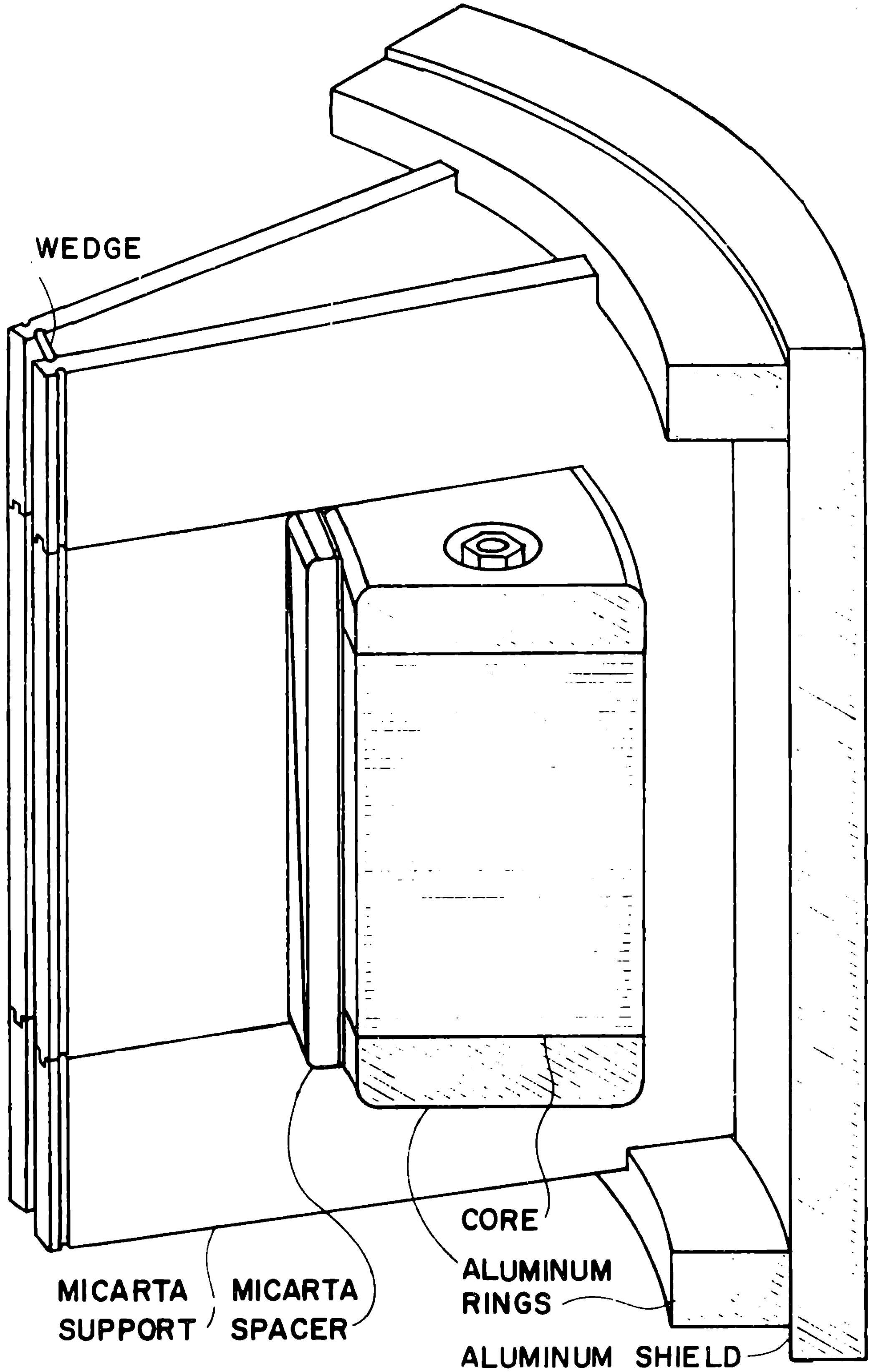

Figure 11: Section Through Armature, Side View

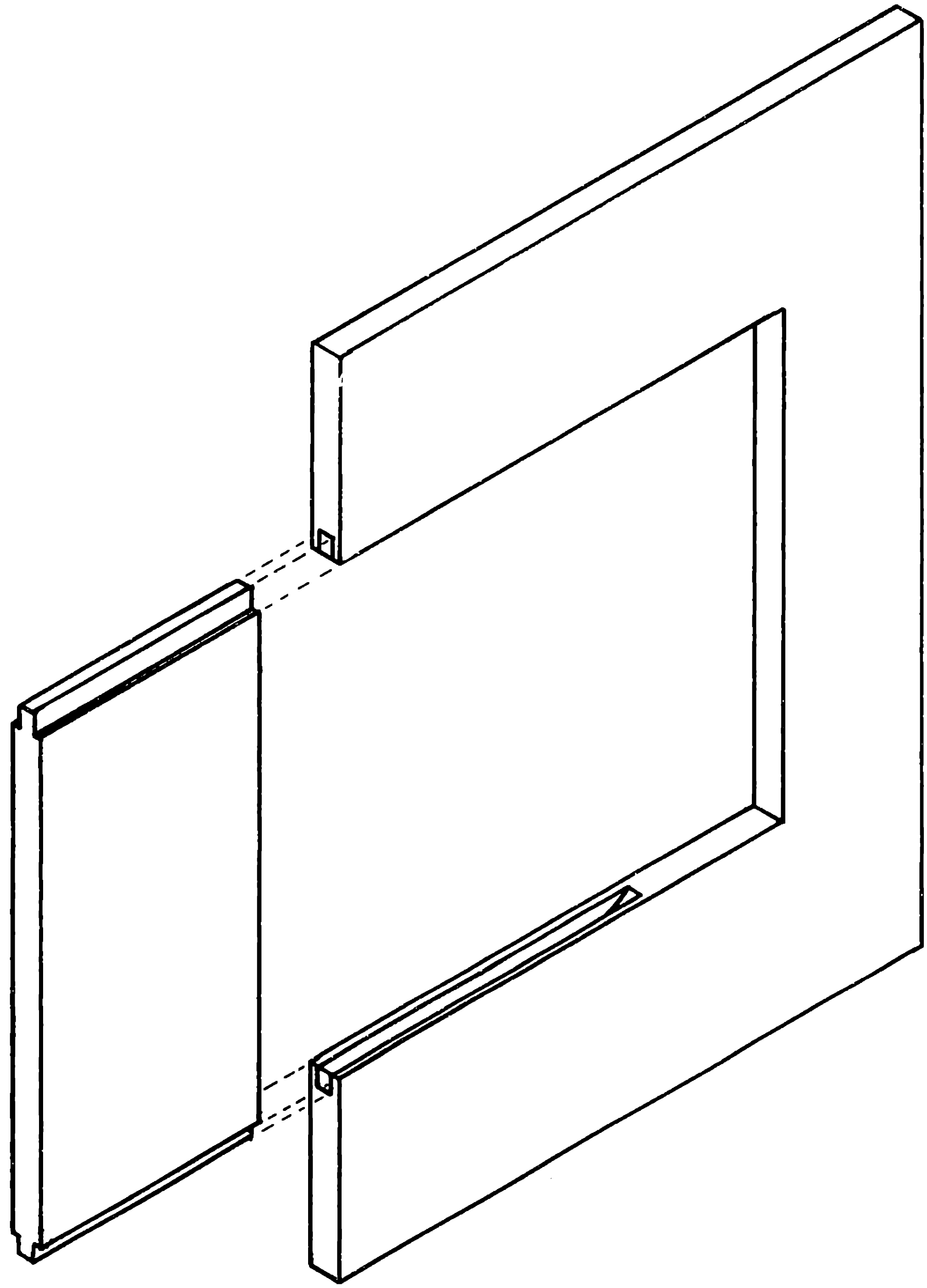

Figure 12: Construction of Armature Supports

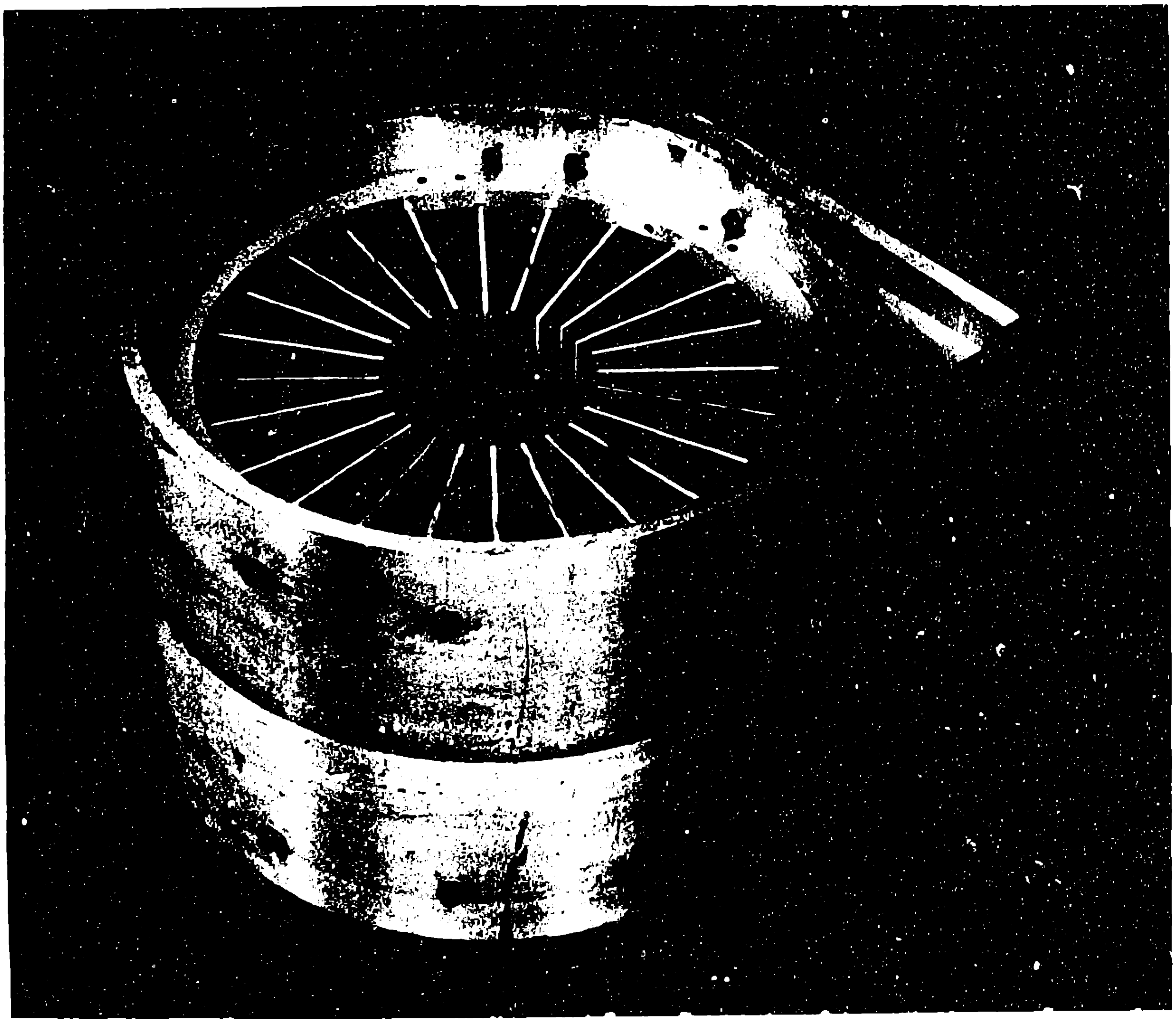

Figure 13: Outer Shield During Construction, Supports in Place

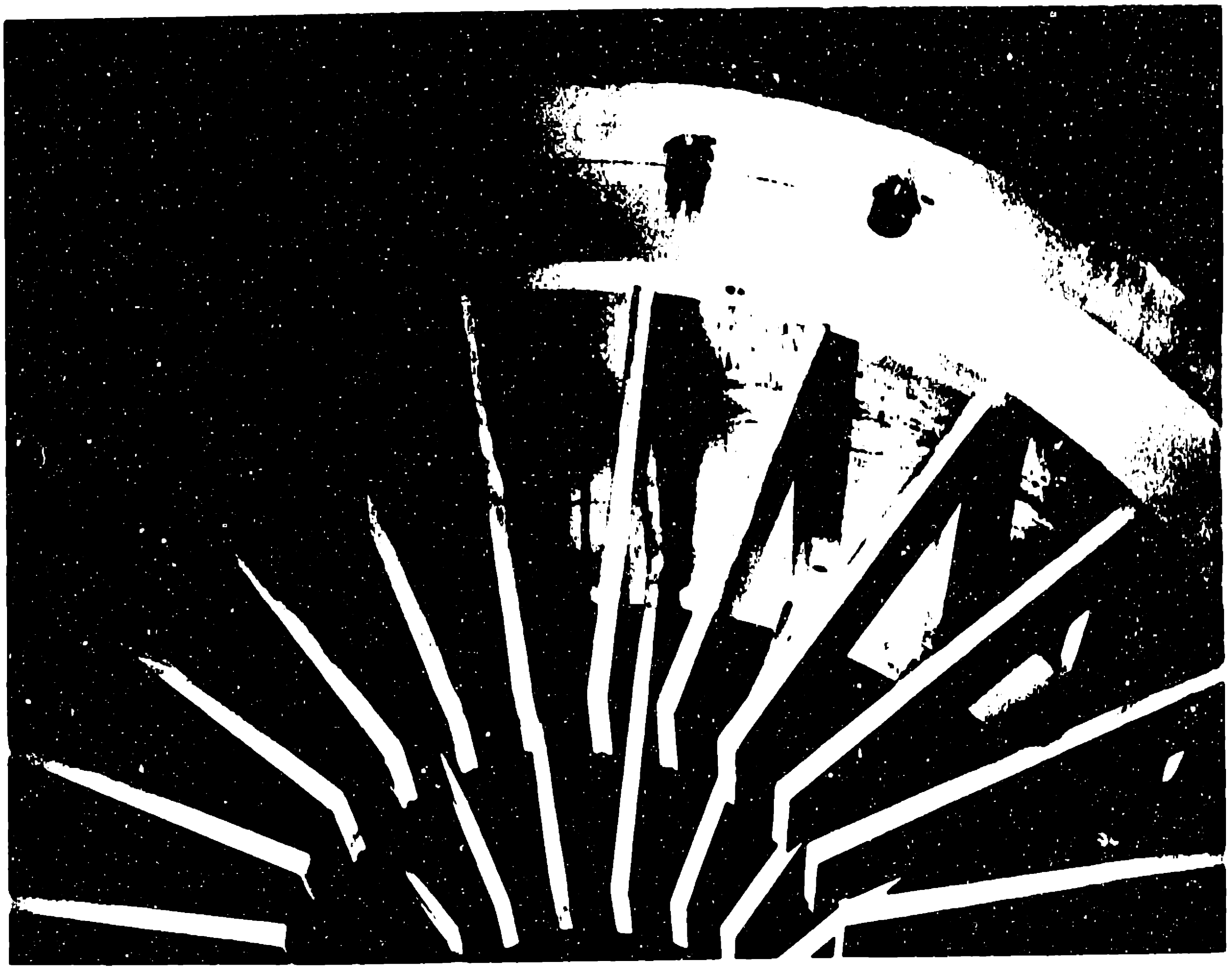

Figure 14: Close-up of Supports

All 24 supports are bonded into a single unit by 24 spacers. Each spacer is cut diagonally so as to be composed of 2 triangular pieces. These pieces are then slid relative to one another until the width of the spacer is appropriate. In order to prevent the squeezing out of all the epoxy from the joint, a piece of filter paper soaked in epoxy is placed in each joint. Between each spacer and the core insulation is a thin piece of micarta, which allows slip between spacer and core due to different thermal expansions. Also, wedges fit into slots machined at the inner edge of each support. They ensure that any armature conductor which somehow becomes loose will not tangle up around the rotor, with diasterous results.

A ring of aluminum is placed on each end of the stator core to shield from axial magnetic fields, which would otherwise induce large eddy current losses in the core. They also serve as compression rings. The core laminations are compressed by four bolts which protrude past the core. The rings have recesses into which the core bolt nuts fit and so provide a smooth surface over which ground insulation is wrapped. The belts are electrically insulated from the laminations and the rings. As previously mentioned ground insulation is wrapped around the core, including the rings. The core assembly just prior to insulating is shown in figure 16. The relative size of the core is apparent from figure 15.

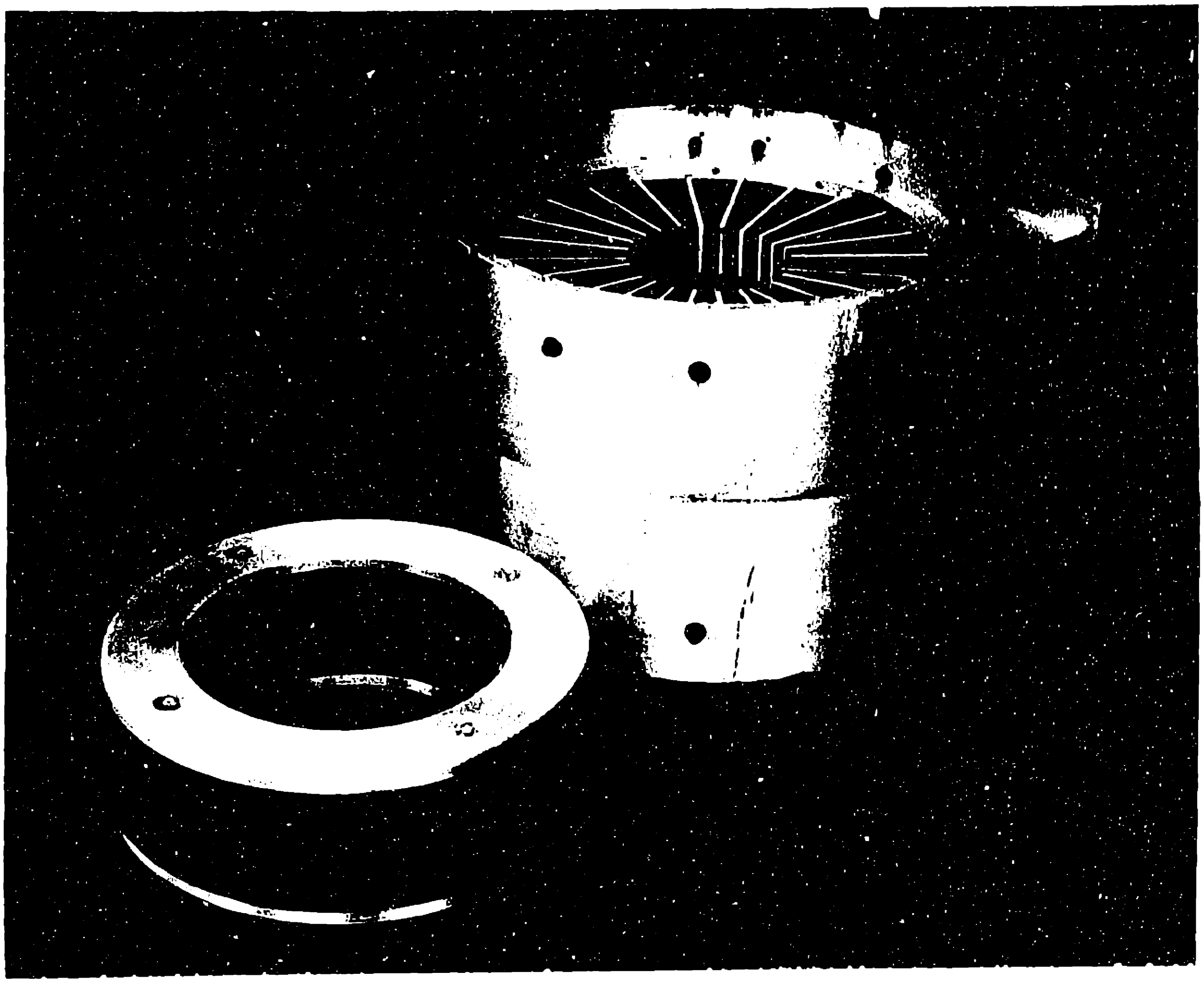

Figure 15: Ferromagnetic Core with its Support Structure

Figure 16: Close-up of Ferromagnetic Core and End Rings

FABRICATION

Special fabrication techniques were needed to efficiently wind the many conductor turns. Since there were about 2200 turns to be applied, the construction of special equipment to speed the process was worthwhile. One piece of equipment constructed was a device to aid in handling the long length of conductor which was to compose one winding. The problem was that as each turn was wrapped around the core, the entire length of wire which had not yet been applied had to be pulled through the center of the core. The solution was a bobbin, a circular holder, shown in figure 17. It is placed around the core, through its center, as shown in figure 18. The length of conductor needed for the winding being constructed is wound on the bobbin. Then the conductor is conveniently fed off the bobbin by rotating it around the core.

The second piece of equipment constructed was a device for pulling the conductor tight down on the core in order to obtain the highest possible packing factor. Simply pulling by hand would not allow sufficient force. The mechanism, shown in figure 19, uses a pair of rubber-lined jaws which clamp down on the conductor harder as the conductor is pulled tighter. This mechanism proved to be successful, although the rubber pads had to be replaced after each winding was completed. In addition, great care was taken to keep the conductors parallel in the inner armature region, the region of smallest volume. This helped obtain a high packing factor.

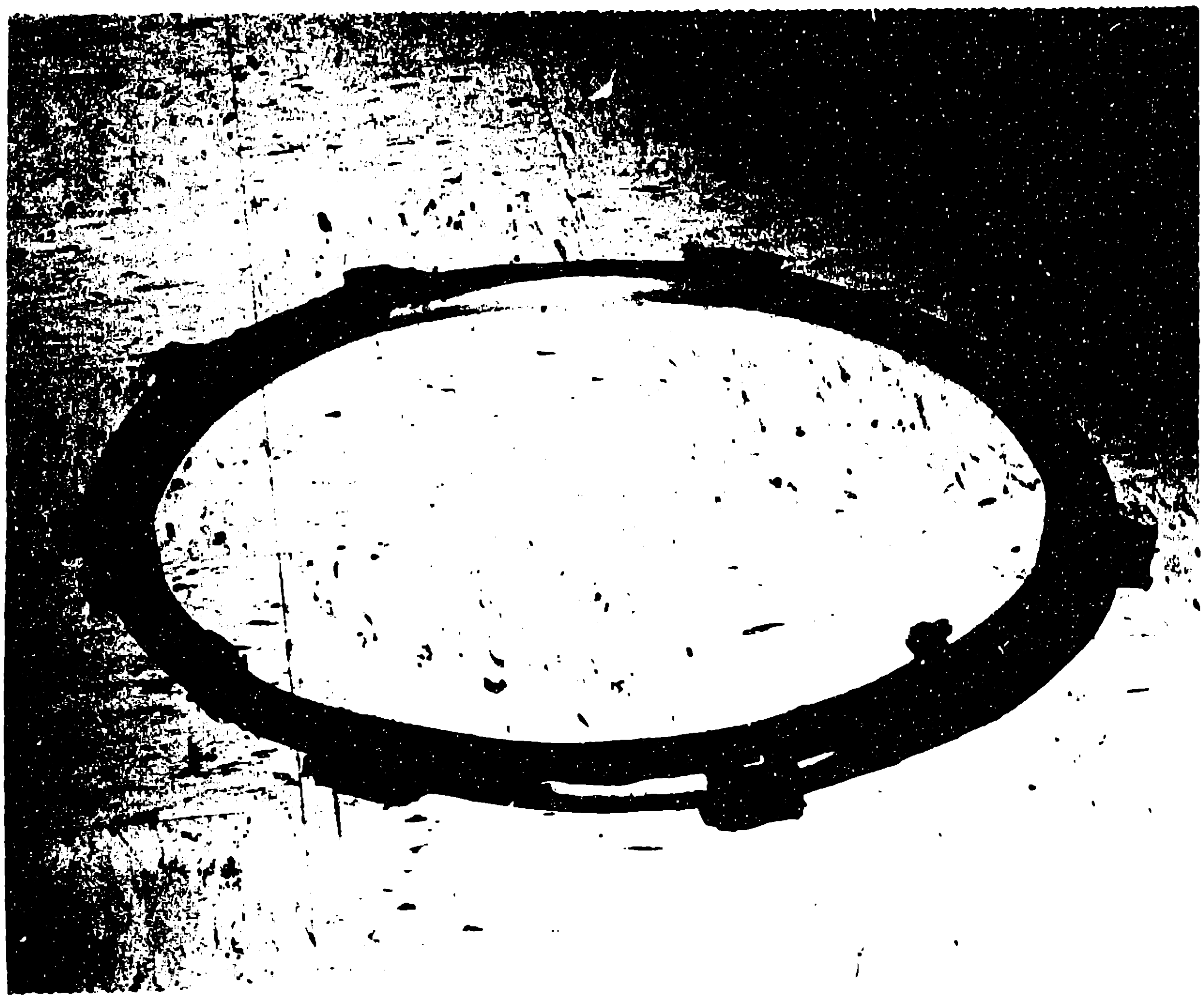

Figure 17: Bobbin

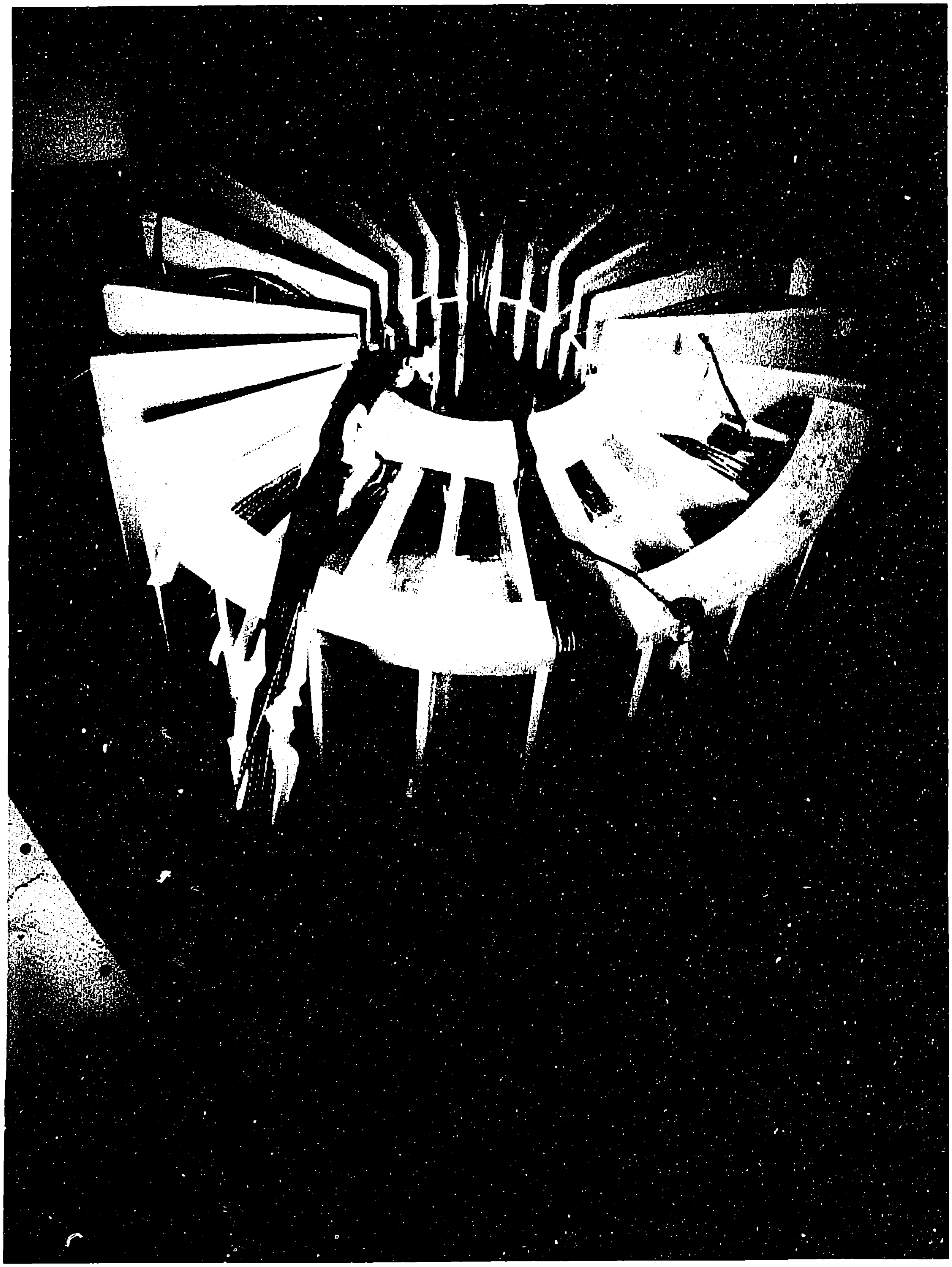

Figure 18: Winding Procedure

The third problem was that as the conductors were pulled tight on the winding being constructed the supports on either side of that winding tended to be forced apart in an azimuthal direction, decreasing the volume available to the adjacent windings. This problem was avoided by constructing aluminum pieces which distribute the force over several adjacent supports and so decrease the displacement. The pieces are illustrated in figure 19, and the winding process in figure 18.

As previously mentioned, ground insulation is wrapped around the core. The insulation used is a polyester and glass filament tape filled with a B-stage epoxy. Upon heating, it first becomes fluid, adheres to all contacted parts, then cures to a tough plastic. Also, the polyester warp fibers shrink, tightening the insulation. This material has the General Electric trade name Fusa-Flex. Four half-lapped layers, equivalent to eight thicknesses, of .007 inch thick Fusa-Flex were applied. Consequently, the maximum voltage gradient within the insulation is limited to 7 volts per mil, less than its dielectric strength.

Fortunately an oven large enough to hold the core was available. The core, wrapped with uncured insulation was placed on a thin teflon sheet and they positioned on a flat surface in the oven. The purpose of the sheet was simply to prevent the core from sticking to the oven surface.

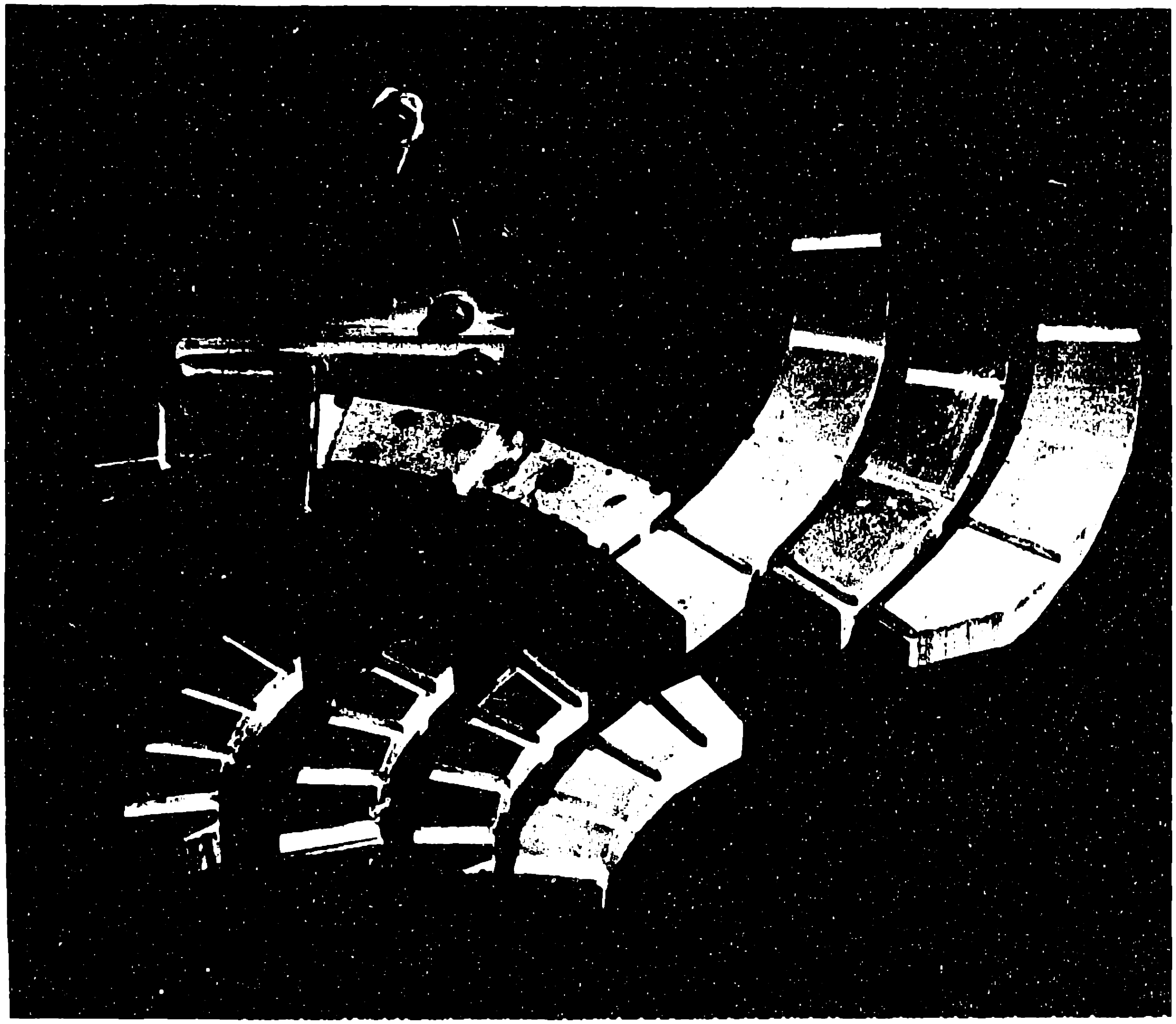

Figure 19: Tools Constructed for Winding Procedure

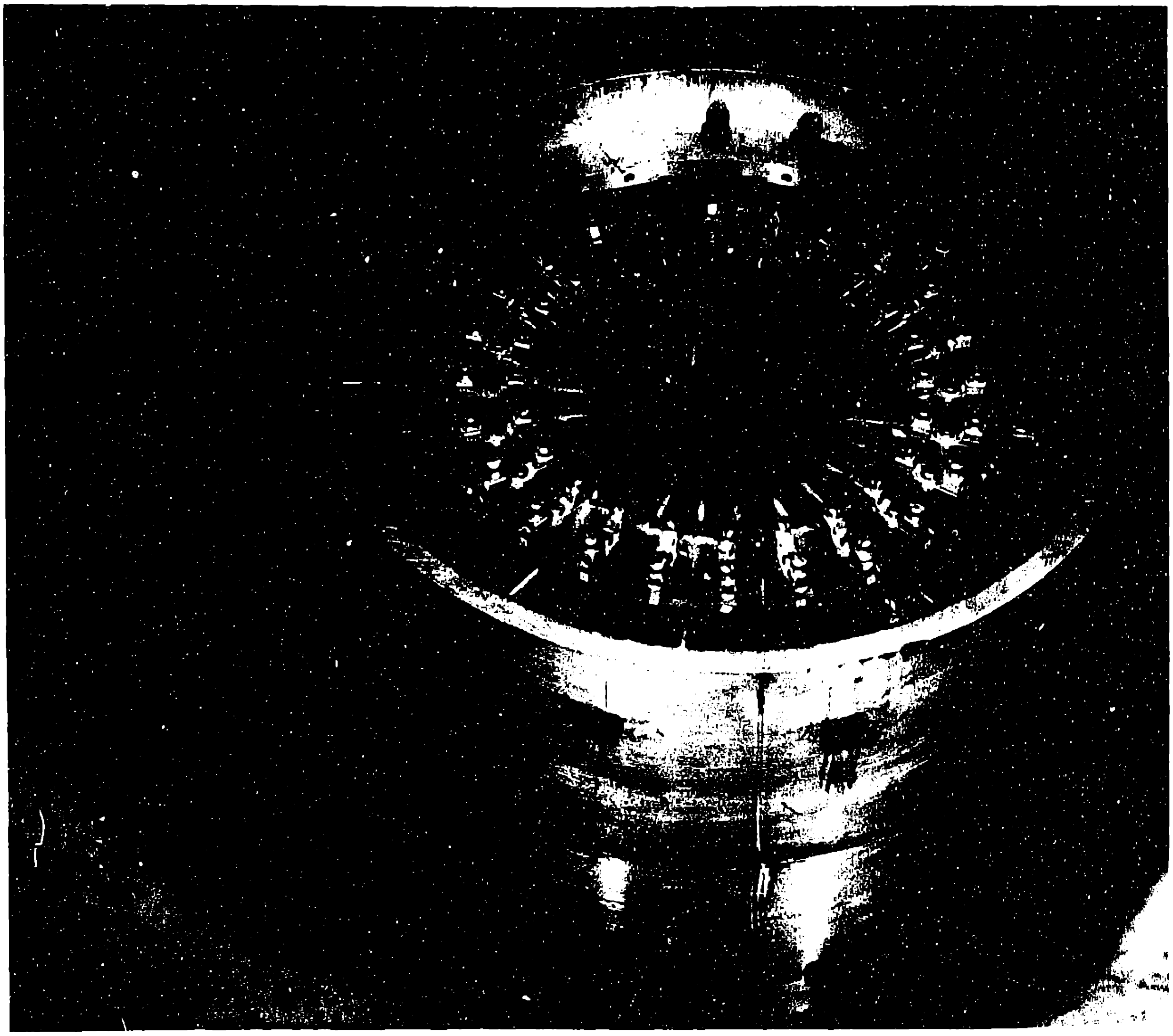

Figure 20: Completed Armature

TEST PROCEDURE

Armature Tests

Measurements were made to determine some of the properties of the armature, without the rotor in place. Except for the D.C. resistance measurement, all measurements were made with a high current 60 Hz source. The D.C. resistance was measured with a standard low current diameter.

The impedance of each phase was measured with both phase belts connected. Only the phase being tested was excited. The A.C. resistance test was performed by exciting all three phases and measuring the dissipated power and current in each phase belt. The self inductance of each phase was then determined by applying the equation

$$L_q = \sqrt{Z^2 - R_{AC}^2}$$

The mutual inductance between phases was measured by exciting one phase and noting the voltage induced in the other phases. To estimate the power loss in the shield, the armature was excited by a known three phase current, and the temperature rise of the shield as a function of time was measured. The increase in temperature was nearly linear with time, indicating that over the small temperature excursion measured (about 10°C) heat transfer from the shield was negligible. Using standard values for heat capacity and density of aluminum, the power loss in the shield at the known armature current was determined from the equation

$$P = \frac{Q}{\Delta\tau} = \frac{\rho C V \Delta t}{\Delta\tau}$$

where Δt is the increase in temperature in an interval of time $\Delta\tau$, ρ is mass density, C is heat capacity, and V is the volume of the shield. It was assumed that the shield was always at a uniform temperature--in other words, that the time required for heat to diffuse to all parts of the shield was much less than the duration of the test. This assumption can be justified by an analysis of the heat conduction equation for isotropic materials.

$$\nabla^2 t = \frac{1}{\alpha}\frac{\partial t}{\partial \tau}$$

Where α is thermal diffusity. A "characteristic" diffusion time τ_c can be found by applying a characteristic length in the following manner.

$$\frac{1}{l_c^2} = \frac{1}{\alpha}\frac{1}{\tau_c}$$

$$\tau_c = \frac{l_c^2}{\alpha}$$

Using the known thermal diffusity of aluminum, and a characteristic length equal to the distance from the farthest axial extent of armature conductors to the farthest axial extent of the shield, we arrive at a characteristic time of about 2 minutes. This is much less than the duration of the measurement, which was about 17 min. Therefore, the duration of the test was appropriate. In addition, it was assumed that the loss in the shield was proportional to armature current squared. This allowed us to calculate the shield loss at rated armature current. This result is included in Table 3.

Generator Tests

Only open circuit and short circuit tests were performed. Figure 21 illustrates the open circuit armature voltage as a function of field current. Figure 22 shows the short circuit armature current versus field current. Figures 23 and 24 show these voltage and current waveforms.

The mutual inductance between the armature and field was calculated by applying results from the open circuit test to the equation

$$E_{f_{LL}} = \frac{\omega M I_f}{2\sqrt{2}}$$

Table 3 lists the result. The power rating was determined by the following procedure.

$$P = 3 V_{LL} I_{ph}$$

where V_{LL} is rated line-to-line terminal voltage and Iph is rated phase current. Further, in reference (8), it is shown that

$$\frac{V_{t_{LL}}}{E_{f_{LL}}} = \sqrt{1 - x_a^2 \cos^2\psi} - x_a \sin\psi$$

where ψ is the power factor angle, assumed to be 31.8°, and the per unit parameter x_a is the synchronous reactance normalized to internal voltage

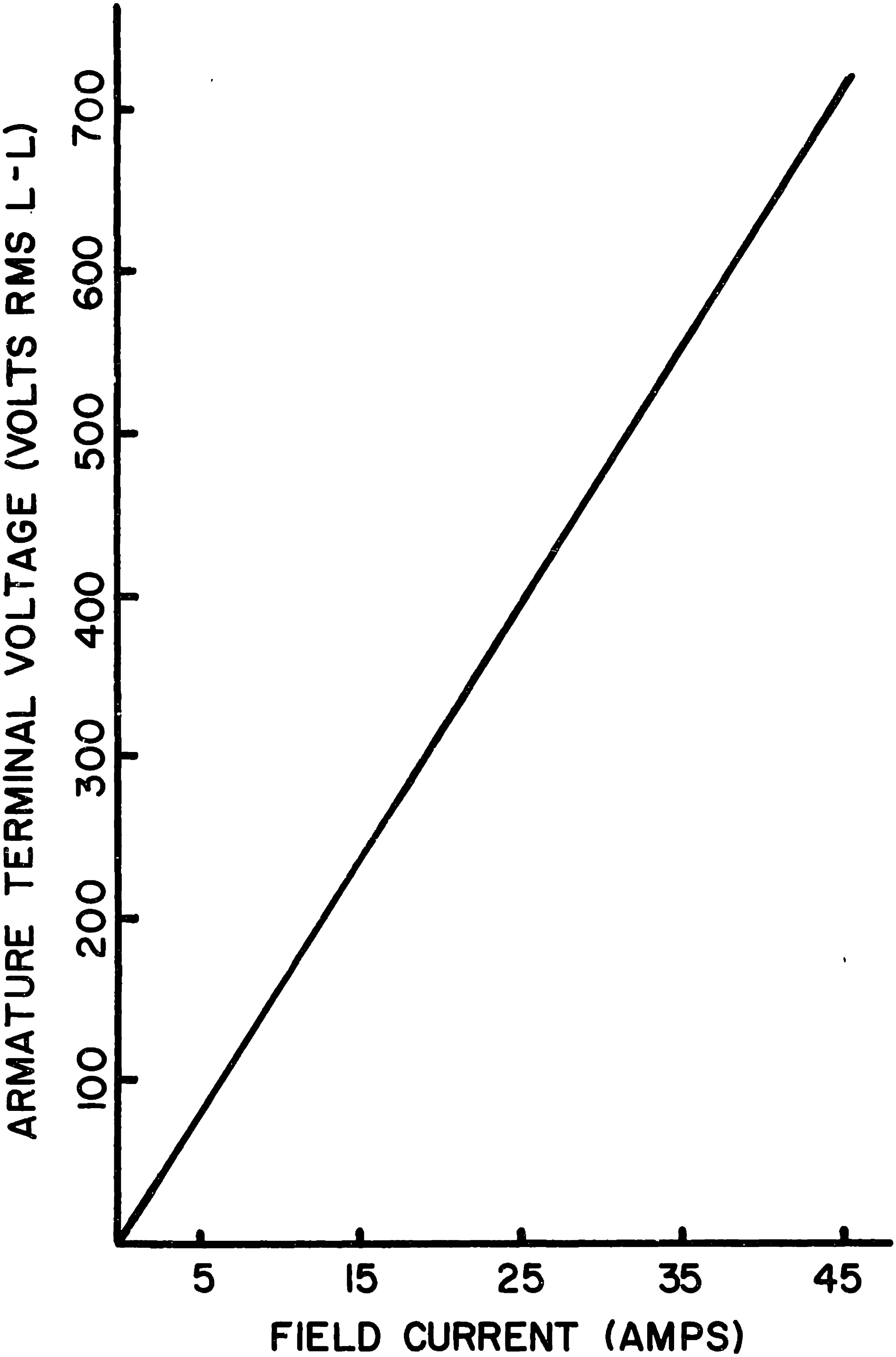

Figure 21: Open Circuit Armature Terminal Voltage Versus Field Current

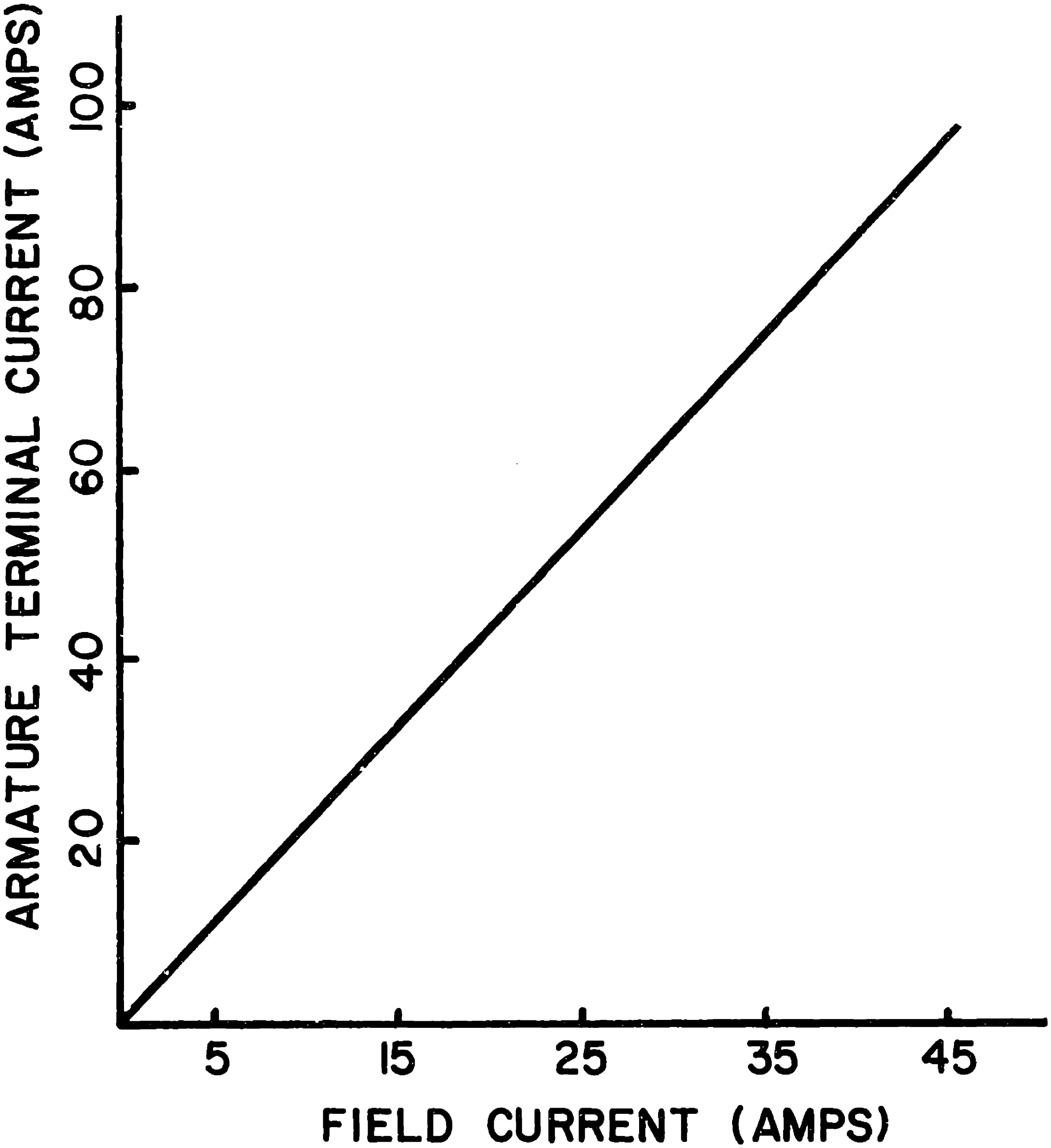

Figure 22: Short Circuit Terminal Current Versus Field Current

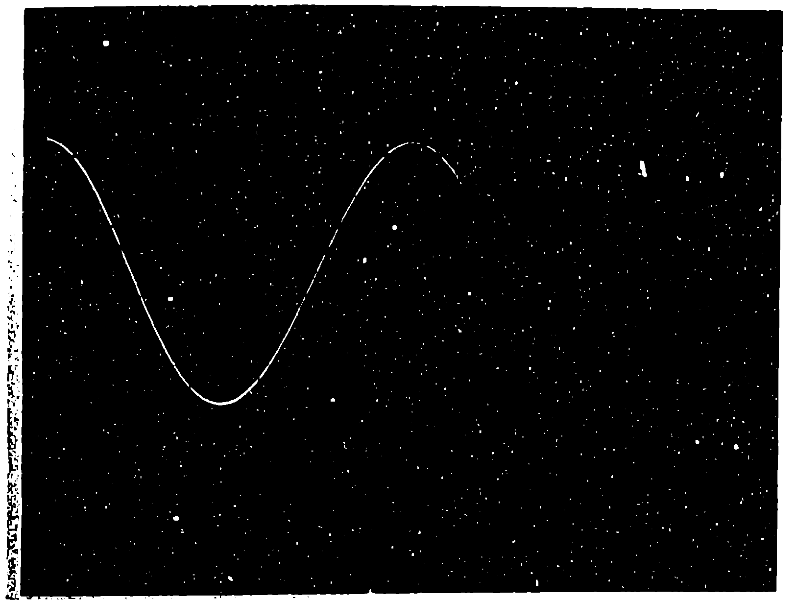

Figure 23: Short Circuit Armature Terminal Current Waveform

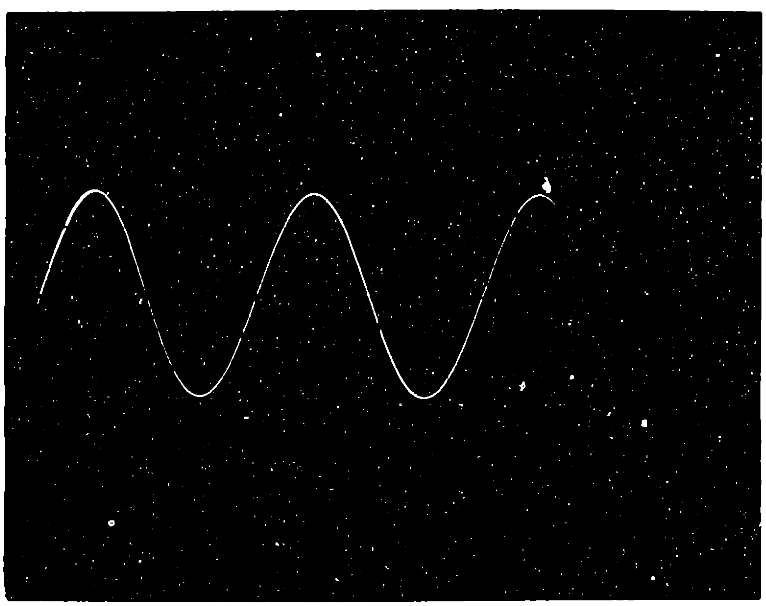

Figure 24: Open Circuit Armature Voltage Waveform

From the ratio of open circuit voltage to short circuit current, X_a the synchronous reactance is determined to be 13.1 ohms per phase (Δ) , or .498 per unit, normalized to internal voltage. Then V_{tLL}/E_{fLL} can be calculated to be .644. Finally, the power rating is determined by

$$P = 3 \frac{V_{tLL}}{E_{fLL}} I_{ph} E_{fLL}$$

to be 37 kVA.

During the open circuit and short circuit tests, measurements of drive motor power were made to determine the losses in the machine. Also, to determine the sum of windage, friction, and D.C. motor losses, the rotor was spun at several speeds with no field current, and the drive power noted. At 3600 rpm this loss was 1087 watts. From these measurements the armature A.C. resistance is determined: the power loss per phase is divided by the square of the phase current. The value obtained is 1.71 ohms per phase (Δ).

These power measurements can be conviently summarized in graph form. Figure 25 indicates the predicted core loss as a function of field current. Figure 26 illustrates the predicted eddy current loss as a function of field current. Figure 27 presents the estimated shield loss as a function of armature current. Now we incorporate measured power loss. Figure 27 presents the estimated shield loss as a function of armature current.

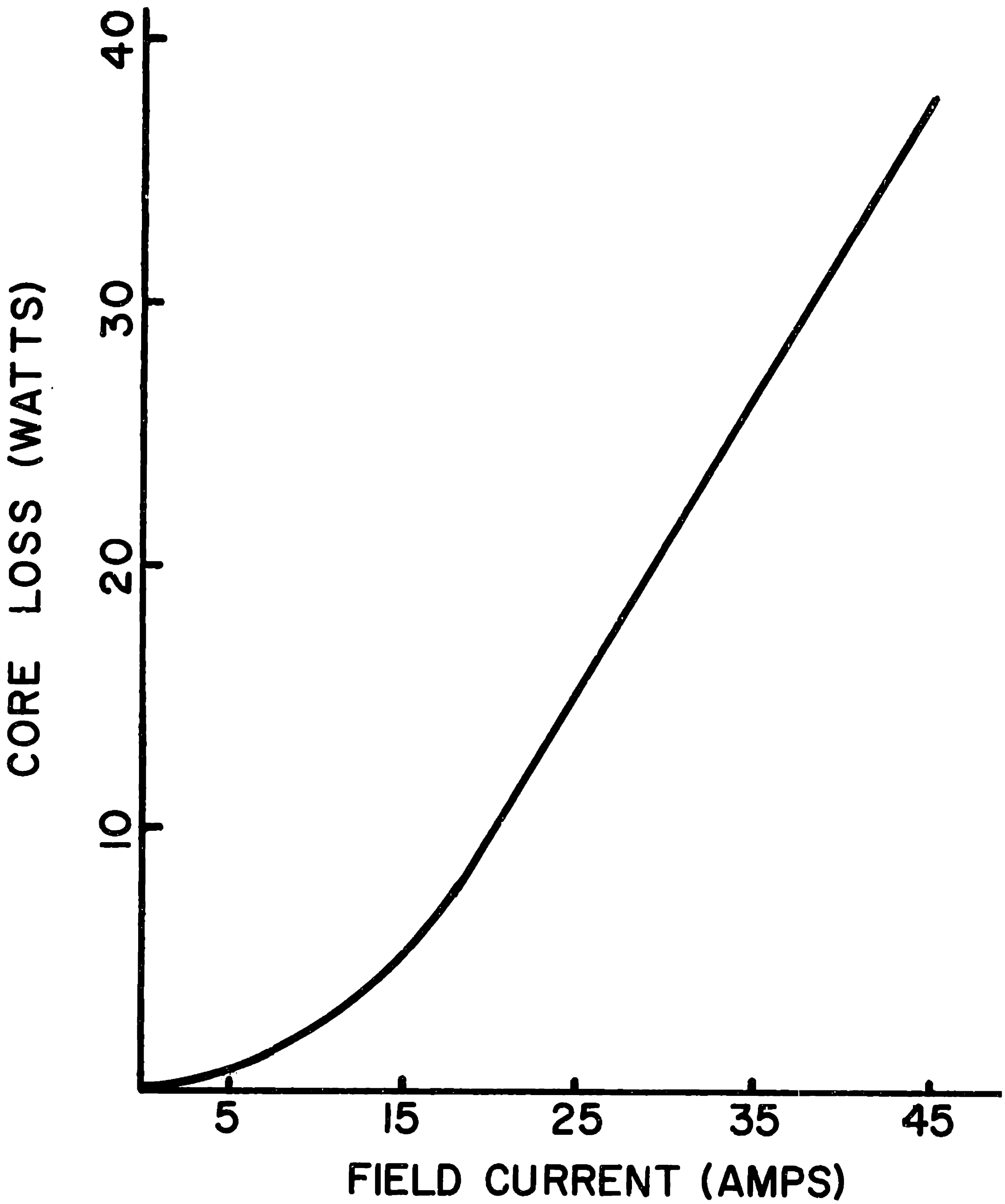

Figure 25: CALCULATED CORE LOSS AT 60 HZ WITH ARMATURE OPEN CIRCUITED

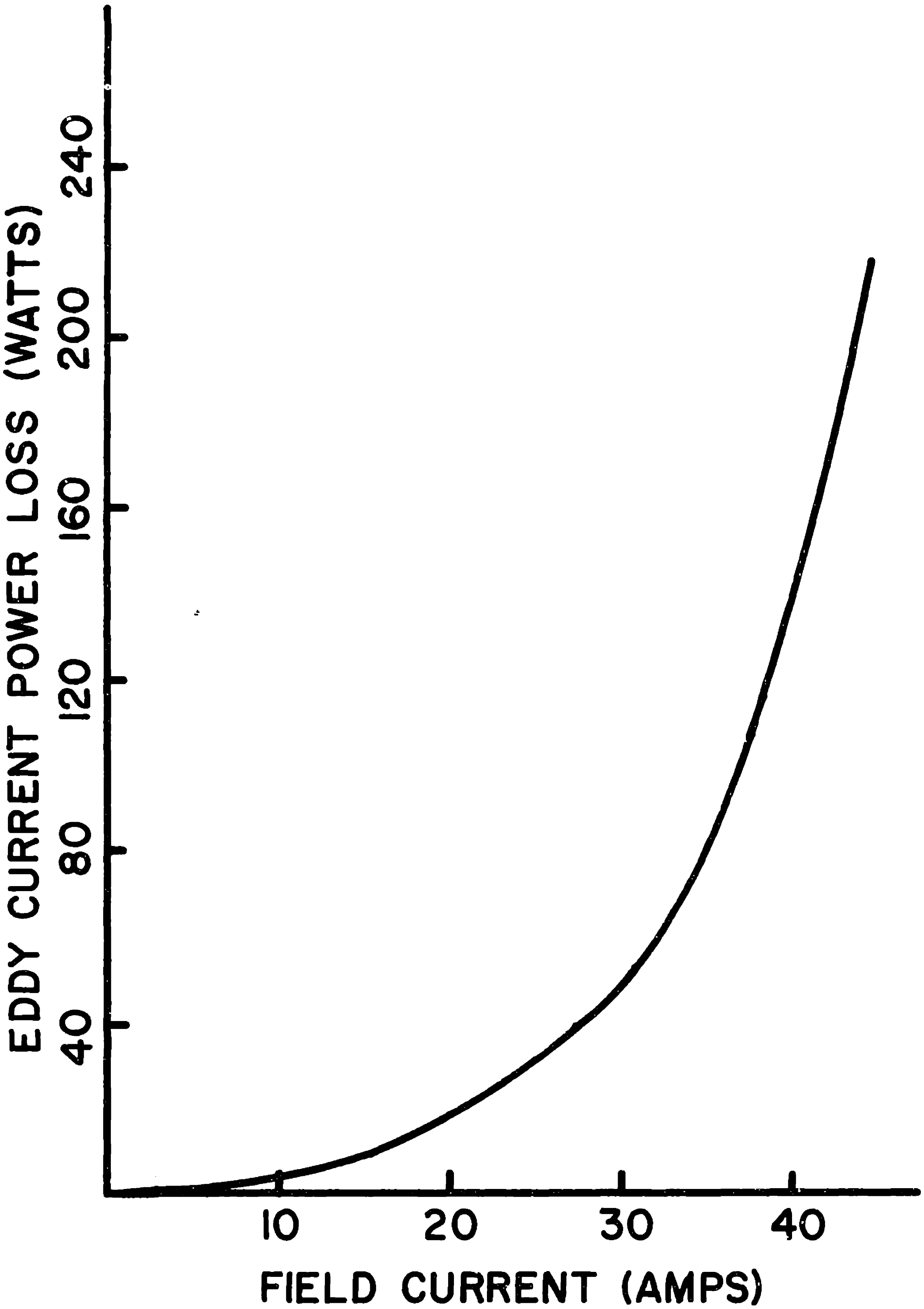

Figure 26: Calculated Eddy Current Loss at 60 Hz with Armature Open Circuited Versus Field Current

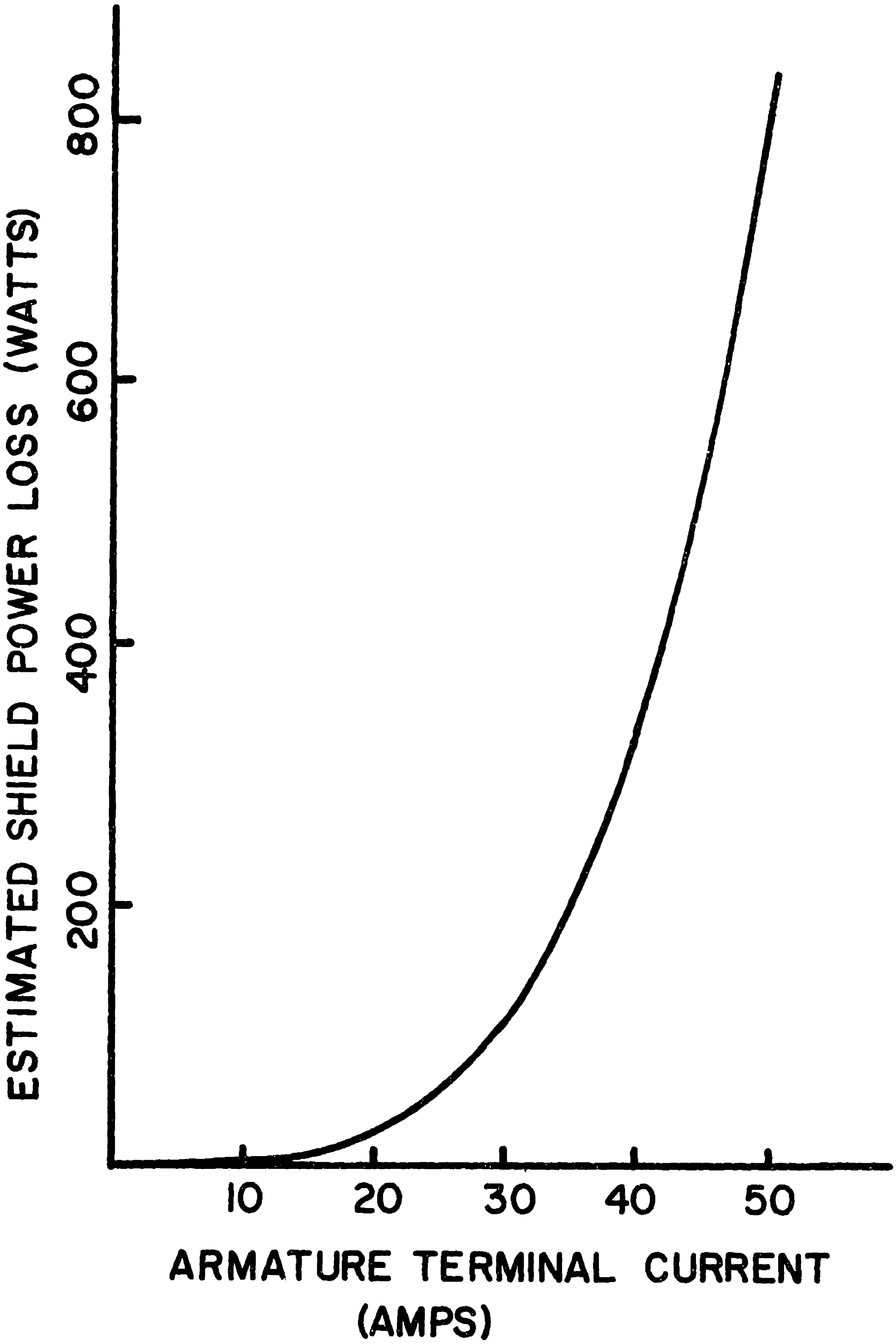

Figure 27: Estimated Shield Loss at 60 Hz versus Armature Terminal Current

Figure 28 shows drive power less windage and friction loss, predicted eddy current loss, and predicted core loss during the open circuit test as a function of field current for two speeds. Figure 29 shows drive power less windage and friction loss, and predicted shield loss during the short circuit test as a function of field current for three speeds.

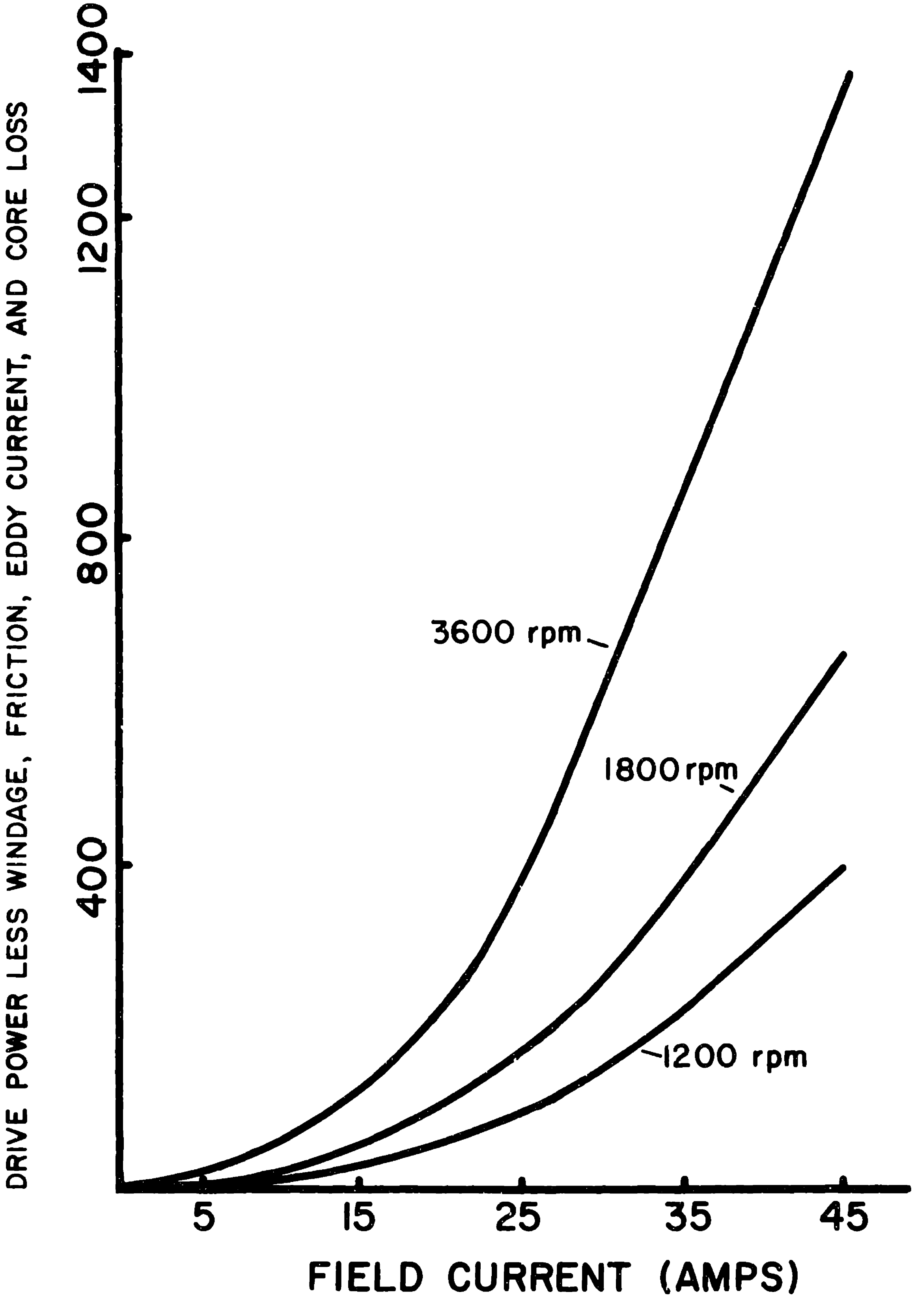

Figure 28: NET DRIVE POWER WITH ARMATURE OPEN CIRCUITED

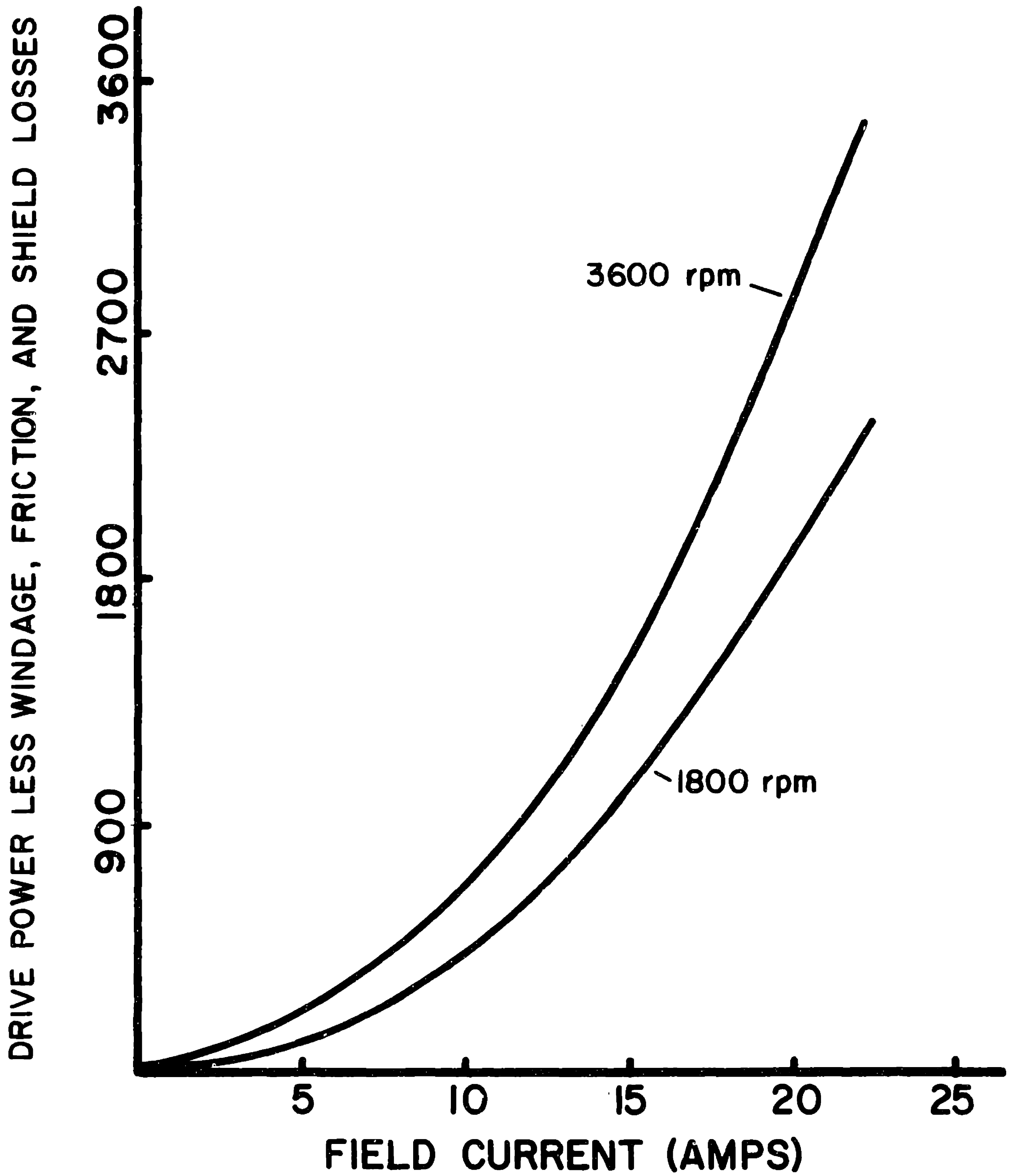

Figure 29: NET DRIVE POWER WITH ARMATURE SHORT CIRCUITED

Table 3

Summary of Results

Parameter	Theoretical Analysis	Armature Test	Generator Test
R_{DC} (ohms per phase Δ)	----	.38	----
R_{AC} (ohms per phase Δ	----	1.96	1.71
L_a (mH per phase Δ	21.3	23.3	----
Lab (mH per phase Δ	-10.6	-8.86	----
M (mH per phase Δ)	128.4	----	118.4
x_d (per unit)	.712	.72	.76
Rated internal voltage (volts rms)	770	----	710
Rated terminal current (amps rms)	46.7	----	----
Eddy current power loss*,*** (watts)	217	----	----
Core power loss*,*** (watts)	37	----	----
Shield power loss** (watts)	834	890	----
Armature D.C. resistance power loss** (watts)	----	831	----
Total short circuit*** (watts)	----	----	3702
Total open circuit losses*** (watts)	----	----	1613
Power rating*** (kVA)	----	----	37
Efficiency (%)	----	----	85.6

* armature open circuited
** at rated, armature current
*** at rated field current

ANALYSIS OF TEST RESULTS

There are many origins of power loss in the armature, including D.C. resistance loss, eddy current loss, circulating current loss, core loss, shield loss, and core ring loss. The relative effectiveness of these sources of loss changes as the armature terminal condition changes. Specifically, when the armature is short circuited, its reaction flux will nearly cancel the field winding flux in the inner armature and core. Hence the circulating current loss, eddy current loss, and core loss will be small. However, other sources of power loss will be significant. Specifically, armature currents flowing across the core rings will set up currents in them. Similarly, outer armature currents will produce currents in the shield. Field winding flux will also induce currents in the shield. However, because the short circuited armature will protect the shield from most field flux, and because the rotor flux density is small at the radius of the shield(5), the losses produced by field flux will be small. So, under short circuit conditions, the significant losses are the D.C. resistance loss, shield loss, and core ring loss.

In contrast, under open circuit conditions the armature produces no flux; consequently, the inner armature is exposed to full field winding flux. In this case, there will of course be no armature D.C. resistance loss. Further, there will be no shield loss due to armature flux. Also, the core will protect the shield from most field flux; therefore, shield losses will be negligible. However field flux will not be shielded from the core or core rings. Field flux will produce core loss and will induce currents in the core rings. (Note that there are two different mechanisms for the generation of currents in the core rings: armature currents under short circuit conditions, and field flux under open circuit conditions.

Considering the above arguments more carefully, we make the following observations. First, because the armature conductors are composed of filaments twisted together with a pitch of about an inch, they are well transposed. Consequently we expect circulating current loss to be low. Further, core loss and eddy current loss have been calculated; armature D.C. resistance has been measured; shield loss has been measured and calculated. For both open and short circuit tests, the only unknown is the core ring loss. This can be found simply by subtracting from the total power loss in the armature all the other terms. Table 4 gives the results of such a calculation.

Table 4

Core End Ring Loss

Power loss, armature o.c. (watts)	1360
Power loss, armature s.c. (watts)	2080

CONCLUSIONS

The performance of this modified Gramme-Ring armature corresponds well with predictions based on a field analysis. Specifically, discrepancies are summarized in Table 5.

Table 5

Comparison of Predictions and Test Results

Parameter	Error (%)
La^*	9
Lab^*	18
M^{**}	8
x_d^*	1
x_d^{**}	7
Open circuit voltage**	8
Shield power loss*	7

* prediction compared with armature test result

** prediction compared with generator test result

Discrepancies are to be expected since the theoretical analysis considers only fundamental fields, whereas the measured values contain contributions from higher order harmonics.

Further, we conclude that armature losses could have been reduced by some slight design changes. First the most striking of the test results is the high power loss in the core rings. This problem could have been reduced by constructing the rings from a more highly conductive material, for example, copper. Nevertheless, further work on this problem appears to be justified; for example, special provision for cooling the rings may be necessary. Second, the shield should be reconsidered, with more importance placed on minimizing power loss. This might be achieved by allowing a larger spacing between the shield and outer armature or by constructing the shield from a material of higher conductivity.

EVALUATION OF CONCEPT

From the results of this experiment, we can conclude that the modified Gramme-Ring armature remains a viable possibility for use in superconducting generators. A theoretical analysis of designs for larger superconducting generators using modified Gramme-Ring armatures has been carried out.

This experiment offers evidence of the validity of this analysis.

APPENDIX I

Losses in Outer Shield

The outer aluminum shield acts as an image shield. That is, its function is to provide a path for currents induced by the alternating magnetic field. The currents will flow in such a direction as to oppose the diffusion of the field through the shield.

In preview, the calculation of losses in the shield will proceed in the following manner. The magnetic diffusion phenomenon is governed by the diffusion equation[9]

$$\frac{1}{\mu\sigma}\nabla^2\bar{B} = \frac{\partial \bar{B}}{\partial t}$$

The magnetic flux density in the aluminum shield will be determined from the solution of this equation with appropriate boundary conditions imposed. The currents will be found by applying Amperes law under the magneto-quasi-static approximation.

$$\bar{J} = \nabla \times \bar{H}$$

The power loss in the shield will then be calculated by integrating the square of the current density over the volume of the shield and multiplying by resistivity.

$$P = \int_V J^2 \rho \, dV$$

Before beginning the calculation, it is noted that the solution of the diffusion equation in cylindrical coordinates involves the introduction of Bessel functions and so becomes complicated. This complication can be avoided by observing that the thickness of the shield is much less than its radius; that is, we assume the solution of the diffusion equation in cylindrical coordinates can be approximated by the solution in cartesian coordinates. Figure A-1 illustrates the result of the transformation to cartesian coordinates; that is, the mental operations of making a cut parallel to the center-line and flattening the formerly cylindrical shield have been performed.

The magnetic field, applied to the shield is modeled as a sinusoidal wave traveling in the x-direction. Further, its wavelength is the length of the shield, denoted by c.

Mathematically,

$$\bar{B} = Re\left[\left(\underline{B}_x(y)\, i_x + \underline{B}_y(y)\, i_y\right) e^{j(\omega t - \beta x)}\right]$$

where $\beta = \frac{2\pi}{\lambda}$ and λ is the "effective" wavelength, c.

$$\beta = \frac{2\pi}{c}$$

Inserting this expression for magnetic flux density into the diffusion equation yields

$$\frac{\partial^2 \underline{B}_y(y)}{\partial y^2} e^{j(\omega t - \beta x)} - (\beta^2 + j\omega\mu\sigma)\underline{B}_y(y)\, e^{j(\omega t - \beta x)} = 0$$

But since

$$\omega = 377$$
$$\mu = \mu_0 = 4\pi \times 10^{-7} \text{ henries/meter}$$
$$\sigma = 3.77 \times 10^{7} \text{ mho/meter}$$
$$\beta = 3.937$$

we find that $\beta^2 << \omega\mu\sigma$. So, the diffusion equation reduces to

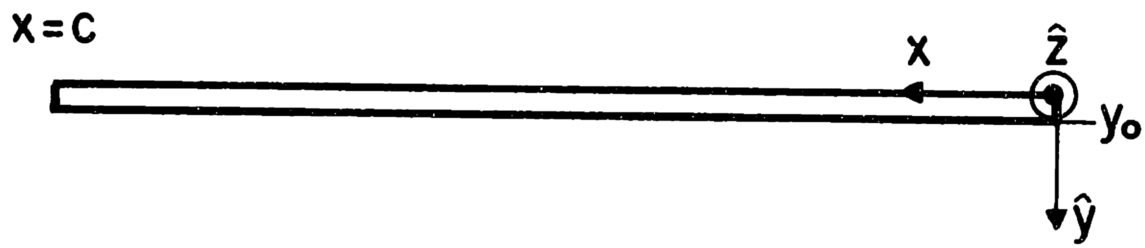

Figure A-1: Flattened Shield

$$\frac{\partial^2 \underline{B}_y(y)}{\partial y^2} - j\omega\mu\sigma \underline{B}_y(y) = 0$$

This has solution

$$\underline{B}_y(y) = \underline{C}_1 e^{\underline{\alpha} y} + \underline{C}_2 e^{-\underline{\alpha} y}$$

where

$$\underline{\alpha}^2 = j\omega\mu\sigma$$

$$\underline{\alpha} = \frac{1+j}{\delta}$$

where δ is the skin depth,

$$\delta = \sqrt{\frac{2}{\omega\mu\sigma}}$$

$\underline{B}_x(y)$ can be found by remembering that the magnetic flux density must be divergenceless

$$\nabla \cdot \overline{B} = 0$$

So,

$$\underline{B}_x(y) = \frac{\underline{\alpha}}{j\beta}\left(\underline{C}_1 e^{\underline{\alpha} y} - \underline{C}_2 e^{-\underline{\alpha} y}\right)$$

We may test the validity of the assumption that the diffusion equation can be solved in cartesian coordinates, instead of cylindrical coordinates. In cylindrical coordinates this equation takes the form[(10)]

$$\frac{1}{\mu\sigma}\left[\frac{1}{r}\frac{\partial}{\partial r}\left(r \underline{B}_r(r) e^{j(\omega t-\theta)}\right) + \frac{1}{r^2}\frac{\partial^2}{\partial\theta^2}\left(\underline{B}_r(r) e^{j(\omega t-\theta)}\right)\right]$$

$$= j\omega \underline{B}_r(r) e^{j(\omega t-\theta)}$$

which reduces to

$$\frac{\partial^2}{\partial r^2}\underline{B}_r(r) + \frac{1}{r}\frac{\partial}{\partial r}\underline{B}_r(r) - \left(\frac{1}{r^2} + j\omega\mu\sigma\right)\underline{B}_r(r) = 0$$

Applying the assumed form

$$\underline{B}_r(r) = \underline{C}_1 e^{\alpha r} + \underline{C}_2 e^{-\alpha r}$$

$$\frac{\partial}{\partial r}\underline{B}_r(r) = \underline{C}_1 \alpha e^{\alpha r} - \underline{C}_2 \alpha e^{-\alpha r}$$

$$\frac{\partial^2}{\partial r^2} B_r(r) = \underline{C}_1 \alpha^2 e^{\alpha r} + \underline{C}_2 \alpha^2 e^{-\alpha r}$$

where, as before, $\alpha = \frac{1+j}{\delta}$. The skin depth is on the order of one centimeter. Therefore $\frac{\partial}{\partial r}\underline{B}_r(r)$ is on the order of 100 times smaller than $\frac{\partial^2}{\partial r^2}\underline{B}_r(r)$ and may be neglected. Then the diffusion equation reduces to

$$\frac{\partial^2}{\partial r^2}\underline{B}_r(r) - \left(\frac{1}{r^2} + j\omega\mu\sigma\right)\underline{B}_r(r) = 0$$

An order of magnitude calculation as above gives

$$\frac{1}{r^2} << \omega\mu\sigma$$

As a result, the diffusion equation in cylindrical coordinates reduces in this case to

$$\frac{\partial^2}{\partial r^2}\underline{B}_r(r) - j\omega\mu\sigma\,\underline{B}_r(r) = 0$$

which is identical to the diffusion equation in cartesian coordinates.

The magnetic flux density in the shield may now be determined by applying the boundary conditions. The problem of finding the boundary conditions may be solved by the use of surface coefficients[11]. But first we must return to cylindrical coordinates by imagining that the shield has been rolled back up to its original shape.

The surface coefficient is defined as the complex ratio

$$\underline{s}(r) = \frac{\underline{H}_r(r)}{\underline{H}_\theta(r)}$$

The surface coefficient at the outer boundary of the shield is $-j$ (11). So, we require that

$$\underline{s} = -j = \frac{j\beta}{\underline{\alpha}} \frac{\underline{C}_1 e^{\underline{\alpha} y_0} + \underline{C}_2 e^{-\underline{\alpha} y_0}}{\underline{C}_1 e^{\underline{\alpha} y_0} - \underline{C}_2 e^{-\underline{\alpha} y_0}}$$

Solving for C_2 in terms of C_1

$$\underline{C}_2 = \underline{a}\,\underline{C}_1$$

where a is $-7.675 + j19.522$

We now determine the second boundary condition. First, using the above result, we can solve for the surface coefficient at the inner surface.

$$\underline{s} = \frac{j\beta}{\underline{\alpha}} \frac{\underline{C}_1 + \underline{C}_2}{\underline{C}_1 - \underline{C}_2} = \frac{j\beta}{\underline{\alpha}} \frac{1 + \underline{a}}{1 - \underline{a}}$$

Second, the surface coefficient at the outer radius of the core is $j\infty$ (11). So, the region between the core and the shield constitutes a cylindrical region with known inner and outer surface coefficients. Therefore, the field produced by the armature can be determined. The radial field due to an infinitesimal current sheet at r=R is (11)

$$\underline{H}_r(r = R_o) = -\frac{j\underline{K}}{2} \left[\frac{1 + \underline{\Gamma}_i \left(\frac{R_i}{R}\right)^2}{1 - \underline{\Gamma}_o \underline{\Gamma}_i \left(\frac{R_i}{R_o}\right)^2} \right] \left(\frac{R}{R_o}\right)^2 \left(1 + \underline{\Gamma}_o\right)$$

where R_i and R_o are the inner and outer radii of the cylindrical region, as shown in figure A-2. $\underline{\Gamma}_i$ and $\underline{\Gamma}_o$ are the inner and outer reflection coefficients defined

$$\underline{\Gamma}_i = \frac{\underline{s}(R_i) - j}{\underline{s}(R_i) + j} \qquad (1)$$

$$\underline{\Gamma}_o = \frac{\underline{s}(R_o) + j}{\underline{s}(R_o) - j} \qquad (2)$$

Using known surface coefficients in (1) and (2),

$$\underline{\Gamma}_i = 1$$

$$\underline{\Gamma}_o = \frac{\frac{j\beta}{\underline{\alpha}} \frac{1+\underline{a}}{1-\underline{a}} + j}{\frac{j\beta}{\underline{\alpha}} \frac{1+\underline{a}}{1-\underline{a}} - j}$$

The total radial H field at $r = R_o$ is the summation over all current sheets

$$\underline{H}_{r_{total}}(r=R_o) = \int_{R_{aio}}^{R_{aoo}} -\frac{j}{2} \left[\frac{1 + \underline{\Gamma}_i \left(\frac{R_i}{R}\right)^2}{1 - \underline{\Gamma}_o \underline{\Gamma}_i \left(\frac{R_i}{R_o}\right)^2} \right] \left(\frac{R}{R_o}\right) \left(1 + \underline{\Gamma}_o\right) \underline{J}_a \, dR$$

where $\underline{J}_a$ dR is substituted for $\underline{K}$ and $\underline{J}_a$ is the complex peak armature current density.

Now, to solve for the second constant of the diffusion equation, we solve the previous equation for the radial magnetic field at the inner surface of the shield and use it as the second boundary condition of the diffusion equation. This results in a value for C_1. That is, the known radial magnetic

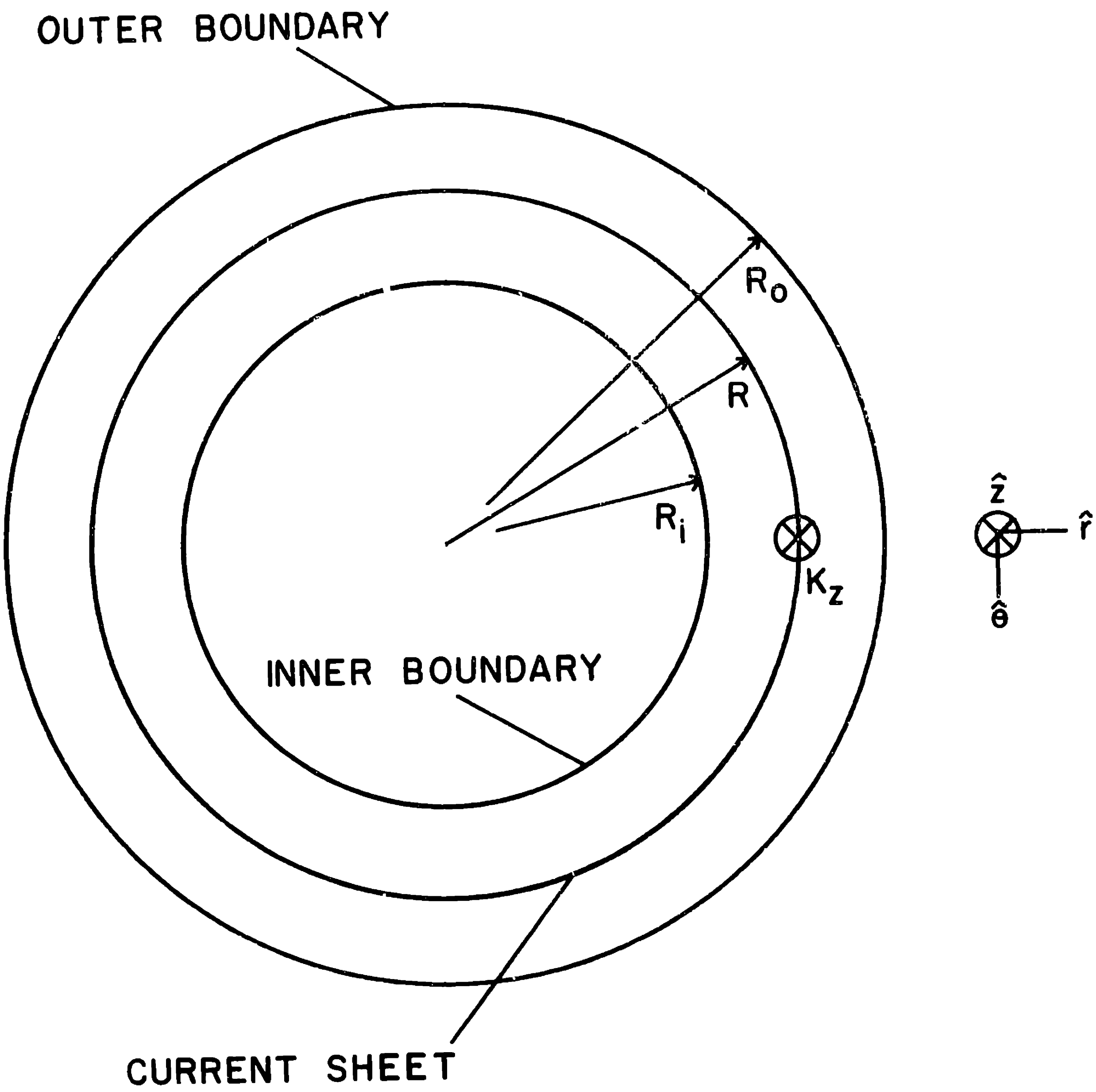

Figure A-2: Field Problem: Azimuthally Traveling Wave of Axial Current With Inner and Outer Concentric Boundary Conditions field applied to the inner surface of the shield, $\underline{H}_{r\,total}(r=R_o)$ may be substituted into the expression for the field within the shield evaluated at the inner surface

$$\mu_o \underline{H}_{r_{total}}(r=R_o) = \underline{B}_y(y=0) = \underline{C}_1 + \underline{C}_2 = \underline{C}_1(1+\underline{a})$$

$\underline{C}_1$ is then found to be $(-4.831 \times 10^{-5} - j\,1.978 \times 10^{-5})\ \mu_o \underline{J}_a$ So, the magnetic flux density in the shield is known.

Following the procedure outlined previously, the currents in the shield are calculated by

$$\bar{J} = \nabla \times \bar{H}$$

or

$$J_z = \frac{\partial}{\partial x} H_y - \frac{\partial}{\partial y} H_x$$

$$\underline{J}_z = -j\beta\,\underline{H}_y(y) - \frac{\partial}{\partial y}\underline{H}_x(y)$$

At this point the current density in the shield is complex. Its magnitude is determined to be

$$|\underline{J}| = \left| \frac{\underline{C}_1}{\mu_o}\left(\beta - \frac{\alpha^2}{\beta}\right)\left(e^{\alpha y} + \underline{a}\,e^{-\alpha y}\right) \right|$$

and is substituted into the expression for time-averaged power loss in the shield

$$P_{sl} = \int_V \frac{|\underline{J}|^2}{2} \rho \, dV$$

Finally, we come to the result

$$P_{sl} = 834 \text{ watts}$$

REFERENCES

1. Kirtley, J.L., Jr., et. al., "Rotating Electric Machine Having a Toroidal Winding Geometry," U.S. Patent Application Ser. No. 372, 129, Filed June 19, 1973.
2. Thullen, P., "Analysis of the Application of Superconductivity to Commercial Electric Power Generation," Sc.D. thesis, Dept. of Mechanical Engineering, MIT, June, 1969.
3. Greene, D.L., "Design of a Superconducting Field Magnet for a Synchronous Generator," N.E. and S.M. thesis, Dept. of Naval Architecture, MIT, May, 1968.
4. Dudley, J.C., "Fabrication of an Armature for a Generator with a Superconducting Field Winding," S.M. thesis, Dept. of Mechanical Engineering, MIT, June, 1969.
5. Thullen, P., Dudley, J.C., Greene, D.L., Smith, J.L, Jr., and Woodson, H.H., "An Experimental Alternator with a Superconducting Field Winding," <u>IEEE Transactions (Power Apparatus and Systems)</u>, vol. PAS-90, no. 2, pp. 611-619, March/April 1971.
6. Steeves, M.M., "A Modified Gramme-Ring Armature for a High Voltage Superconducting Alternator," S.M. thesis, Dept. of Electrical Engineering, MIT, August, 1973.
7. Steeves, M.M., Kirtley, J.L., Jr., "Toroidal Winding Geometry for High Voltage Superconducting Alternators," <u>IEEE Transactions (Power Apparatus and Systems)</u>, vol. PAS-93, no. 6, pp. 1902-1908, November/December, 1974.

8. Kirtley, J.L., Jr., "Design and Construction of an Armature for an Alternator with a Superconducting Field Winding," Ph.D. thesis, Dept. of Electrical Engineering, MIT, August, 1971.

9. Woodson, H.H., and Melcher, J.R. Electromechanical Dynamics, Wiley, New York, 1968.

10. Luck, D.L., "Electromechanical and Thermal Effects of Faults Upon Superconducting Generators," Ph.D. thesis, Dept. of Electrical Engineering, MIT, June 1971.

11. Kirtley, J.L., Jr. "Surface Coefficient for Multipole Magnetic Field Boundary Condition Problems," IEEE Transactions (Power Apparatus and Systems), vol. PAS-94, no. 3, pp. 934-938, May/June 1975.

12. Smith, J.L., Jr., Kirtley, J.L., Jr., Thullen, P. Woodson, H.H., "MIT-EEI Program on Large Superconducting Synchronous Machines," Proceedings of the 1972 Applied Superconductivity Conference, May 1-3, Annapolis, Maryland, IEEE Publication No. 72CH0682-5-TABSC, pp. 145-150.